Robots Driven by Compliant Actuators: Optimal Control under Actuation Constraints

David J. Braun*, *Member, IEEE*, Florian Petit, Felix Huber, Sami Haddadin, *Member, IEEE*, Patrick van der Smagt, *Member, IEEE*, Alin Albu-Schäffer, *Member, IEEE* and Sethu Vijayakumar

***Abstract*—Anthropomorphic robots that aim to approach human performance agility and efficiency are typically highly redundant not only in their kinematics but also in actuation. Variable-impedance actuators (VIAs), used to drive many of these devices, are capable of modulating torque and impedance (stiffness and/or damping) simultaneously, continuously and independently. These actuators are, however, non-linear and assert numerous constraints, e.g., range, rate and effort limits on the dynamics. Finding a control strategy that makes use of the intrinsic dynamics and capacity of compliant actuators for such *redundant, non-linear and constrained* system is non-trivial. In this work, we propose a *framework for optimization of torque and impedance profiles* in order to maximize task performance, tuned to the complex hardware and incorporating the *real-world actuation constraints*. Simulation study and hardware experiments: i) demonstrate the effects of actuation constraints during impedance control, ii) show applicability of the present framework to simultaneous torque and temporal stiffness optimization under constraints imposed by real-world actuators and iii) validate the benefits of the proposed approach under experimental conditions.**

***Index Terms*—Variable Impedance Actuation, Optimal Impedance Control, Redundant Robots, Dynamics.**

I. Introduction

Modern anthropomorphic robots, aiming to approach human behaviour and performance are highly *redundant*, not only in their kinematics but also *actuation* (e.g., DLR Hand-Arm System [1], see Fig.1). Variable impedance actuators (VIAs) [2]–[9], used to drive many of these devices are capable of *simultaneous torque and passive impedance (i.e., stiffness and/or damping) modulation* as opposed to more classic actuators on torque controlled robots [10]. The premise of impedance control [11] and the variable impedance actuation paradigm is to increase the performance i.e., dynamic range, agility and safety of robots [12]–[17]. This however does not come for free. Indeed, VIAs introduce non-linearities by design, employ multiple motors per joint, and assert important actuation constraints: range, rate and effort limitations, that are often neglected on classical devices. Due to these reasons, the potential offered by variable impedance actuation may only be exploited if the control problem at hand is *algorithmically treated* and if the control redundancy is *optimally resolved* in a task specific manner [18]. However, there are number of challenges to this:

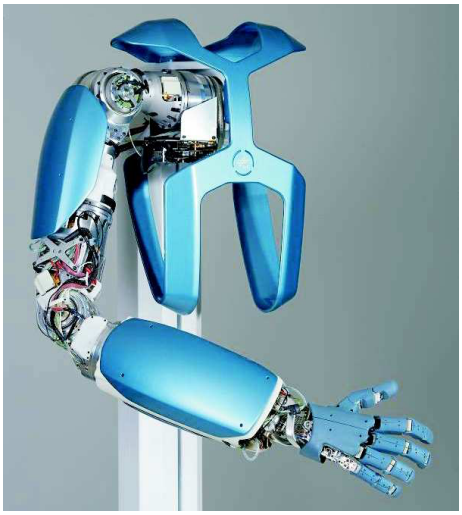

Fig. 1. The DLR Hand-Arm System resembles the complexity of a human upper limb. This device has 26 kinematic degrees of freedom all driven by variable stiffness actuators. These actuators incorporate 52 motors.

- First, it is known that the model structure of a compliantly actuated robot is more complex than that of rigid robots, and as such, *it is often non-trivial to find the right representation of the dynamics: that is neither too complex to be computationally intractable nor too simple to lack validity with respect to the real physics of the system.*

One of the widely used models of *elastic-joint robots*, with constant joint stiffness, was derived by Spong [19]. In this model, the trade-off between complexity and physical validity was balanced by neglecting the inertial coupling between the motor and the link-side dynamics. This was shown to be viable under highly geared actuation. If this design condition is not provided, one may be required to work with a more general model, as the one introduced by Tomei [20]. There is considerable interest to provide extensions for such models

David J. Braun and Sethu Vijayakumar are with the School of Informatics, University of Edinburgh, United Kingdom.

Florian Petit, Felix Huber, Sami Haddadin and Alin Albu-Schäffer are with the German Aerospace Centre (DLR), Institute of Robotics and Mechatronics, Oberpfaffenhofen-Weßling, Germany.

Patrick van der Smagt is affiliated with the Institute for Informatics, Technische Universität München.

This work has been funded by the European Commission's Seventh Framework Programmes as part of the STIFF (grant number 231576) and VIACTORS (grant number 231554) projects and the Sixth Framework Programme as part of the SAPHARI (grant number 287513) project. The authors also acknowledge the support of the DLR Hand-Arm System design team.

Part of this paper was presented at the IEEE/RSJ International Conference on Intelligent Robotic Systems, Algarve, Portugal, October 2012.

This paper has supplementary downloadable video (48 MB) available at http://ieeexplore.ieee.org which demonstrates the proposed framework implemented on two conceptually different variable stiffness devices.

*Address correspondence to: DJB, E-mail: david.braun@ed.ac.uk

for systems with *variable joint elasticity*. To this end, there are various formulations derived using Spong's assumption and by assuming "arbitrarily fast" dynamics of stiffness modulation.

In Section II, we propose a general model for compliantly actuated robots driven with series-elastic and variable-stiffness actuators (i.e., SEAs [21] and VSAs [8]) that: i) incorporates the inertial coupling between the rigid body and the motor dynamics, ii) is valid for (physically and/or geometrically) non-linear, redundantly actuated systems and iii) in the case of VSAs, includes the real dynamics associated with stiffness modulation. As derived, this model generalizes those frequently used for elastic joint robots, while it also extends representations of variable stiffness systems recently presented in the literature [22]–[24]. Based on this model, we propose a *physically consistent minimalistic representation* of the dynamics for optimal control planning. In Section VII, this representation is tested (and shown to be viable) for complex variable stiffness robots performing dynamic movements.

- Second, it is of interest to find a suitable control strategy that enables *exploitation of the natural dynamics of the system through utilization of the intrinsic compliance of the actuators.*

The control literature of elastic joint robots having constant joint stiffness contains various approaches, especially to the *position control* problem [25]. Among these are the: singular perturbation-based approaches [26], decoupling-based approaches [19], [27], backstepping-based schemes [28] and the passivity-based approaches [29], [30] to mention a few. In the same context, combined *position and stiffness control* of variable stiffness robots is more recently investigated using (a decoupling-based) feedback linearizion [31], [32]. These approaches generally combine *closed-loop motor position and velocity control* with *link-side feedback* on positions, torques and their derivatives. Using the former, one compensates the uncertainties in the motor dynamics, while using the latter one may track desired link-side position (and stiffness) trajectories.

In the present paper, we assume that the model of the system dynamics is reasonably well identified; either using standard system identification [33] or on-line learning [34], [35]. Under this assumption, we investigate an approach to *open-loop elastic torque and stiffness modulation*. In this formulation (Sections III and IV), the link-side motion is not preplanned and tracked in a traditional sense, but instead it is a consequence of the mechanical properties of the link-side dynamics and the output of the compliant actuators. This output is provided by the elastic torques and stiffness that is continuously modulated through an optimally planned *motor program*. This motor program is implemented through motor position and velocity feedback. Accordingly, we employ active feed-back control to gain robustness with respect to uncertainties in the motor dynamics, while relying on the mechanical feed-back at the link-side dynamics provided by the physical compliance of the actuators[1]. It is important to note that using variable impedance actuators, this physical compliance is not fixed but can be optimally modulated during the motion. This allows one to fit the intrinsic properties of the system to the task requirement, that in turn enables better exploitation of the system dynamics during the movement.

- Third, it is vital to employ *algorithmic methods* that can, in a unified way, treat the non-linear coupling between motion, torque and impedance characteristics inherent to systems driven with compliant actuators, and that allow *planning impedance control strategies under real-world actuation constraints.*

One way to define the desired impedance is through the optimal control formulation, where the control task is encoded by an objective functional [37]. Using this idea, it was demonstrated how impedance adaptation can decrease the energy required for movement generation [38] and how impedance optimization can be used to enhance safety in human-robot interactions [14]. Along this line of research, the benefit of *temporal impedance optimization*, and accordingly impedance modulation during movement, have also been recently investigated [16], [17], [24], [39]–[41]. In this context, using algorithmic tools was recognized as especially important since VIAs introduce *non-linear coupling* between motion, torque and impedance characteristics, *actuation redundancy* (increased dimensionality of the control inputs) and *actuation constraints* (range, rate, acceleration limits introduced in Section V). These make heuristic methods less effective when used in planning and control on compliantly actuated systems.

In Section VI, we consider planning optimal impedance control strategies under *actuation constraints* [42], [43]. While analytical approaches may have limitations for constrained problems, there are numerical methods that can be effective in this context [44], [45]. To this end, we provide a systematic treatment of constraints on robotic systems by explicitly embedding non-linear state inequality constraints into the dynamics. In this way the number of state constraints may either be reduced or even fully eliminated from the consideration. As a result, state constraints, that would otherwise require problem specific derivation and sophisticated computation, become easier to treat numerically. In Section VII, we demonstrate the viability of this framework in simulations and hardware experiments. The material presented in the last two sections is an extended exposition of our previous work [24].

In summary, we present a model-based constrained optimal control framework, realizing (variable) impedance control tuned to the task and specificity of the system dynamics. The promise of this framework is applicability to complex, compliantly actuated robots that perform dynamic tasks under real-world conditions.

II. Model of a compliantly actuated robot

In this Section, we present a dynamic model for compliantly actuated robotic systems. In this model, the classical rigid body dynamics of the robot is supplemented with the model of the compliant actuators. These compliant actuators can be: series elastic (SEA) [21] or variable stiffness (VSA) [8] with no restriction on generality.

[1]This is unlike *active stiffness control* (e.g., [36]) realized through link-side position feedback on torque controllable devices.

A. Robot dynamics

Consider an n degree-of-freedom autonomous robotic system, the configuration of which is uniquely specified by $\mathbf{q} \in \mathbb{R}^n$ generalized coordinates (e.g., joint angles). Let this system be equipped with m compliant actuators (e.g., SEAs and/or VSAs), and let $\boldsymbol{\theta} \in \mathbb{R}^m$ ($m \geq n$) denote the motor angles reflected through gear reduction, see Fig.2. In the remainder of this paper we refer to $\mathbf{q}$ and $\boldsymbol{\theta}$ as *link-side* and *motor-side* coordinates respectively.

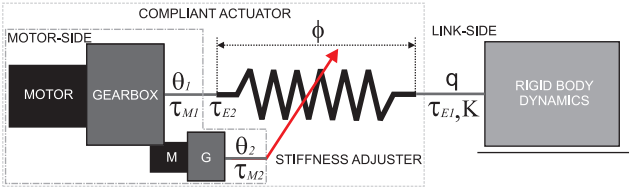

Fig. 2. Schematic representation of a compliantly actuated robot: $\boldsymbol{\theta}$ – motor positions, $\boldsymbol{\tau}_M$ – motor torques, $\boldsymbol{\phi}$ – spring length, $\boldsymbol{\tau}_{E2}$ – motor-side elastic torques, $\boldsymbol{\tau}_{E1}$ – link-side elastic torques, $\mathbf{K}$ – link-side stiffness of the actuators, $\mathbf{q}$ – link positions.

Due to standard geometric features we assume that:

A.1 the rotation axes of the motors and gearboxes, that drive these actuators, are axes of symmetry and correspondingly they coincide with the *principal axes of inertia*[2].

Based on (A.1), we next define the *kinetic and the gravitational potential energy* of the rigid body dynamics and the dynamics of the motors. In addition, we also define the *elastic potential energy* to characterize the elastic torques/forces generated by the actuators. Using these energy functions, the *equation of motion* of the compliantly actuated system is derived through application of the Lagrangian formalism [47].

1) Kinetic energy: Under assumption A.1, the kinetic energy of the considered dynamical system reads

$$\mathcal{T} = \underbrace{\frac{1}{2}\dot{\mathbf{q}}^T\mathbf{M}(\mathbf{q})\dot{\mathbf{q}}}_{\mathcal{T}_{11}(\mathbf{q},\dot{\mathbf{q}})} + \underbrace{\dot{\mathbf{q}}^T\mathbf{S}(\mathbf{q})\dot{\boldsymbol{\theta}}}_{\mathcal{T}_{12}(\mathbf{q},\dot{\mathbf{q}},\dot{\boldsymbol{\theta}})} + \underbrace{\frac{1}{2}\dot{\boldsymbol{\theta}}^T\mathbf{J}\dot{\boldsymbol{\theta}}}_{\mathcal{T}_{22}(\dot{\boldsymbol{\theta}})}, \tag{1}$$

where $\mathbf{M} \in \mathbb{R}^{n\times n}$ is the symmetric and positive definite inertia matrix of the rigid body dynamics (and the translational dynamics of the actuators), $\mathbf{S} \in \mathbb{R}^{n\times m}$ represents the inertial coupling between the rigid body and the motor dynamics while $\mathbf{J} \in \mathbb{R}^{m\times m}$ is a constant and diagonal matrix that contains the inertia of the motors/gearboxes. In the relation above, the inertial coupling between the link-side and the motor-side dynamics is represented by $\mathcal{T}_{12}$. This term exist since the rotational kinetic energy of each motor/gearbox assembly is not only due their self-rotation, but also due to the rotation of the actuators induced by the motion of the robot.

2) Gravitational potential energy: Under the assumption A.1, the center of mass of the actuators will not change due the self-rotation of the rotors and the gears. This practically means that the center of mass of the composed system does not depend on $\boldsymbol{\theta}$. Direct implication of this is that the gravitational potential energy of the entire system only depends on the configuration of the rigid body dynamics

$$\mathcal{U}_G = \mathcal{U}_G(\mathbf{q}). \tag{2}$$

3) Elastic potential energy: In the present paper, we consider series elastic and variable stiffness actuators where:

A.2 the actuator compliance is provided by *elastic* elements (i.e., linear and/or non-linear springs).

Under this (fairly general) assumption, the *conservative* elastic forces by the actuators can be characterized with a potential energy function[3]

$$\mathcal{U}_E = \mathcal{U}_E(\mathbf{q},\boldsymbol{\theta}) = -\sum_{i=1}^{p}\int_{l_{i0}}^{l_i(\mathbf{q},\boldsymbol{\theta})} F_i(s)ds, \tag{3}$$

where l_i and l_{i0} denote the length and equilibrium length of the i^{th} spring while $F_i = F_i(l_i)$ is the corresponding spring force, $F_i(l_{i0}) = 0$. In the following, we employ (3) to define the elastic torques provided by the compliant actuators.

4) Equation of motion: Using the Lagrangian formalism, the equation of motion of the robotic system becomes

$$\begin{bmatrix}\mathbf{M} & \mathbf{S}\\ \mathbf{S}^T & \mathbf{J}\end{bmatrix}\begin{bmatrix}\ddot{\mathbf{q}}\\ \ddot{\boldsymbol{\theta}}\end{bmatrix} + \begin{bmatrix}\mathbf{C} & \mathbf{C}_q\\ \mathbf{C}_\theta & \mathbf{0}\end{bmatrix}\begin{bmatrix}\dot{\mathbf{q}}\\ \dot{\boldsymbol{\theta}}\end{bmatrix} + \begin{bmatrix}\mathbf{D}\dot{\mathbf{q}}\\ \mathbf{D}_\theta\dot{\boldsymbol{\theta}}\end{bmatrix} + \begin{bmatrix}\mathbf{G}\\ \mathbf{0}\end{bmatrix} = \begin{bmatrix}\boldsymbol{\tau}_{E1}\\ \boldsymbol{\tau}_{E2}\end{bmatrix} + \begin{bmatrix}\mathbf{0}\\ \boldsymbol{\tau}_M\end{bmatrix} \tag{4}$$

where the inertia matrix is defined by $\mathbf{M} = \partial\mathcal{T}^2/\partial\dot{\mathbf{q}}^2$, $\mathbf{S} = \partial\mathcal{T}^2/\partial\dot{\mathbf{q}}\partial\dot{\boldsymbol{\theta}}$ and $\mathbf{J} = \partial\mathcal{T}^2/\partial\dot{\boldsymbol{\theta}}^2$, while

$$\mathbf{C}\dot{\mathbf{q}} = \mathbf{C}(\mathbf{q},\dot{\mathbf{q}},\dot{\boldsymbol{\theta}})\dot{\mathbf{q}} = \frac{\partial^2(\mathcal{T}_{11}+\mathcal{T}_{12})}{\partial\dot{\mathbf{q}}\partial\mathbf{q}}\dot{\mathbf{q}} - \frac{\partial\mathcal{T}_{11}}{\partial\mathbf{q}}, \tag{5}$$

$$\mathbf{C}_q\dot{\boldsymbol{\theta}} = \mathbf{C}_q(\mathbf{q},\dot{\mathbf{q}})\dot{\boldsymbol{\theta}} = -\frac{\partial\mathcal{T}_{12}}{\partial\mathbf{q}}, \tag{6}$$

$$\mathbf{C}_\theta\dot{\mathbf{q}} = \mathbf{C}_\theta(\mathbf{q},\dot{\mathbf{q}})\dot{\mathbf{q}} = \frac{\partial^2\mathcal{T}_{12}}{\partial\dot{\boldsymbol{\theta}}\partial\mathbf{q}}\dot{\mathbf{q}}, \tag{7}$$

$$\mathbf{G} = \mathbf{G}(\mathbf{q}) = \frac{\partial\mathcal{U}_G}{\partial\mathbf{q}}, \tag{8}$$

$$\boldsymbol{\tau}_{E1} = \boldsymbol{\tau}_{E1}(\mathbf{q},\boldsymbol{\theta}) = -\frac{\partial\mathcal{U}_E}{\partial\mathbf{q}}, \tag{9}$$

$$\boldsymbol{\tau}_{E2} = \boldsymbol{\tau}_{E2}(\mathbf{q},\boldsymbol{\theta}) = -\frac{\partial\mathcal{U}_E}{\partial\boldsymbol{\theta}}, \tag{10}$$

where $\mathbf{C} \in \mathbb{R}^{n\times n}$, $\mathbf{C}_q \in \mathbb{R}^{n\times m}$ and $\mathbf{C}_\theta \in \mathbb{R}^{m\times n}$ are matrices that represent the Coriolis and normal inertial forces, $\mathbf{D}\dot{\mathbf{q}} \in \mathbb{R}^n$ and $\mathbf{D}_\theta\dot{\boldsymbol{\theta}} \in \mathbb{R}^m$ are the forces due viscous friction (may be derived using the virtual work principle), $\mathbf{G} \in \mathbb{R}^n$ are the gravitational forces, $\boldsymbol{\tau}_{E1} \in \mathbb{R}^n$ are the elastic joint torques that affect the rigid body dynamics, $\boldsymbol{\tau}_{E2} \in \mathbb{R}^m$ contains the elastic reaction torques at the actuators *input* that affects the motor dynamics, while $\boldsymbol{\tau}_M \in \mathbb{R}^m$ are the motor torques. Accordingly, the first term in (4) represents the *link-side dynamics*, while the second term corresponds to the *motor-side dynamics*.

[2]This is a standard assumption for models of *elastic-joint robots*, see [19], [20], [46] (assumption A.2 in these references).

[3]If the elastic elements are *linear* springs, $F_i = k_i(l_i - l_{i0})$, then (3) simplifies to

$$\mathcal{U}_E(\mathbf{q},\boldsymbol{\theta}) = \frac{1}{2}(\mathbf{l}(\mathbf{q},\boldsymbol{\theta}) - \mathbf{l_0})^T\mathbf{K}_s(\mathbf{l}(\mathbf{q},\boldsymbol{\theta}) - \mathbf{l_0}),$$

where $\mathbf{l}(\mathbf{q},\boldsymbol{\theta}) = [l_1, l_2, ..., l_p]^T$ is the length of the springs, $\mathbf{l_0} = [l_{01}, l_{02}, ..., l_{0p}]^T$ are the equilibrium lengths, while $\mathbf{K}_s = \text{diag}\{[k_{s1}, k_{s2}, ..., k_{sp}]\}$ is a diagonal matrix containing the stiffness constants of the springs.

As derived, equation (4) provides a general model of a compliantly actuated robot. In particular, it extends the model of *elastic joint robots* proposed in [20], since: it remains valid for *redundantly actuated* systems (i.e., $m \geq n$) and is applicable to robots having *non-linear* and *variable* joint elasticity. Compared to the model proposed for variable stiffness robots in [24], (4) accommodates the inertial coupling between the motors and the link-side dynamics (and as such it remains valid even if the motor gearing is not particularly high). Compared to the model proposed in [23], (4) is derived for a generic compliant actuators with no assumption on the physical/geometric non-linearities it introduces to the system.

III. On motor position control of compliantly actuated systems

In the present paper, we investigate an approach to *feed-forward elastic torque and stiffness modulation*. In this approach, the elastic joint torques given by (9) and the associated joint stiffness (defined in Section IV-B) are optimally modulated through a *motor program*. This motor program is defined by the desired motor trajectories that are implemented through *closed-loop control* introduced below.

A. The closed-loop motor dynamics

According to the full model (4), (7) and (10), the actuator dynamics is defined by

$$\mathbf{J}\ddot{\boldsymbol{\theta}} = \boldsymbol{\tau}_M \underbrace{-\mathbf{S}^T(\mathbf{q})\ddot{\mathbf{q}} - \mathbf{C}_\theta(\mathbf{q},\dot{\mathbf{q}})\dot{\mathbf{q}} - \mathbf{D}_\theta\dot{\boldsymbol{\theta}} + \boldsymbol{\tau}_{E2}(\mathbf{q},\boldsymbol{\theta})}_{\boldsymbol{\tau}_\theta(\mathbf{q},\dot{\mathbf{q}},\ddot{\mathbf{q}},\boldsymbol{\theta})}, \quad (11)$$

where $\mathbf{J} = \mathbf{n}^2\mathbf{J}_m$, $\mathbf{J}_m \in \mathbb{R}^{m\times m}$ is a diagonal matrix containing the rotational inertia of the motors and gearboxes (at the *input* to the gear reducers), $i \in \{1,2,...,m\}$, $\mathbf{n}^2 = \mathrm{diag}\{n_i^2\} \in \mathbb{R}^{m\times m}$ are the squared gear ratios while $\boldsymbol{\tau}_\theta \in \mathbb{R}^m$ denotes the inertial effects from the link dynamics and the reaction torques by the compliant elements that affect the actuators.

In order to perform *motor position control*, we employ the following control law

$$\boldsymbol{\tau}_M = -\hat{\boldsymbol{\tau}}_\theta - \mathbf{n}^2\mathbf{K}_m(\boldsymbol{\theta} - \boldsymbol{\theta}_d) - \mathbf{n}^2\mathbf{B}_m\dot{\boldsymbol{\theta}}, \quad (12)$$

where the feed-forward component $\hat{\boldsymbol{\tau}}_\theta$ is the estimate of $\boldsymbol{\tau}_\theta$ in (11), $\mathbf{K}_m = \mathrm{diag}\{k_{mi}\} \in \mathbb{R}^{m\times m}$ and $\mathbf{B}_m = \mathrm{diag}\{b_{mi}\} \in \mathbb{R}^{m\times m}$ are the user-defined (servo) gains while $\boldsymbol{\theta}_d = \boldsymbol{\theta}_d(t) \in \mathbb{R}^m$ is the desired motor position. By substituting (12) into (11), the *closed-loop motor dynamics* becomes

$$\ddot{\boldsymbol{\theta}} + 2\boldsymbol{\beta}\dot{\boldsymbol{\theta}} + \boldsymbol{\kappa}^2\boldsymbol{\theta} = \boldsymbol{\kappa}^2\boldsymbol{\theta}_e, \quad (13)$$

where $\boldsymbol{\beta} = \frac{1}{2}\mathbf{J}_m^{-1}\mathbf{B}_m$, $\boldsymbol{\kappa} = \mathbf{J}_m^{-1}\mathbf{K}_m$ while $\boldsymbol{\theta}_e$ is the *motor equilibrium position* defined by

$$\boldsymbol{\theta}_e = \boldsymbol{\theta}_d + (\mathbf{n}^2\mathbf{K}_m)^{-1}\Delta\boldsymbol{\tau}_\theta, \quad (14)$$

and $\Delta\boldsymbol{\tau}_\theta = \boldsymbol{\tau}_\theta - \hat{\boldsymbol{\tau}}_\theta$. Following the above relation, we can define three conditions under which the actuator dynamics may *not* be (significantly) affected by link-side motion (i.e., state dependent torques included in $\boldsymbol{\tau}_\theta$, see (11)). Indeed, *if*:

- C.1 the inertial torques and the elastic reaction torques are well identified: $\hat{\boldsymbol{\tau}}_\theta \approx \boldsymbol{\tau}_\theta \Rightarrow \Delta\boldsymbol{\tau}_\theta \approx \mathbf{0}$;
- C.2 the motors operate through high gear reduction: $\min\{n_1, n_2, ..., n_m\} \gg 1$;
- C.3 the control torques (12) are realized with high position gains: $\min\{k_{m1}, k_{m2}, ..., k_{mm}\} \gg 1$,

then the last term in (14) becomes negligible i.e., $\boldsymbol{\theta}_e \approx \boldsymbol{\theta}_d(t)$, and the actuator model, (13) and (14), simplifies to

$$\ddot{\boldsymbol{\theta}} + 2\boldsymbol{\beta}\dot{\boldsymbol{\theta}} + \boldsymbol{\kappa}^2\boldsymbol{\theta} = \boldsymbol{\kappa}^2\boldsymbol{\theta}_d. \quad (15)$$

The first condition (C.1) requires precise system identification of the motor-side dynamics that may or may not be provided. On the other hand, high gear reduction (C.2) is often used on robotic systems, and a high position gain (C.3) is a standard attribute of any servo-control system. Accordingly, we assume that at least one of the latter two conditions is satisfied, and as such (15) is a valid representation of the closed-loop motor dynamics[4].

Regarding the choice of the parameters in (15) we note that: i) critical-damping i.e., $\boldsymbol{\beta} = \boldsymbol{\kappa}$ leads to the fastest response without overshoot and ii) servo-control i.e., $\forall\kappa_i \gg 1$ leads to $\boldsymbol{\theta} \approx \boldsymbol{\theta}_d$ independent of the specificity of the motor side dynamics (11). In Sections VI-A and VI-E we will invoke both of these arguments to ensure that the constraint consistent motor program $\boldsymbol{\theta}_d$ leads to optimal constraint consistent motor trajectories $\boldsymbol{\theta}$, irrespective of the motor-side dynamics (11).

It is of interest to note at this point that highly geared motor units (C.2) and/or servo-control (C.3) *do not* cancel out the intrinsic link-side dynamics of the robot on compliantly actuated systems. This is because the compliance of the (SE and VS) actuators effectively *decouples* the link-side from the motor-side dynamics. This is *in contrast* to rigid actuators, where bandwidth limitations on the servo-controlled motor dynamics directly limits the speed/acceleration of the link-side motion. Moreover, this decoupling is the reason why identification of the *link-side dynamics* i.e., the first equation in (4), is easier on compliantly actuated systems than on their rigidly actuated counterparts[5]. This makes adequate system identification and correspondingly feed-forward elastic torque/stiffness modulation viable on series elastic and variable impedance systems e.g., [18], [24].

IV. Model of a compliant actuator

In this section, we propose a general representation of compliant, series elastic and variable stiffness actuators where the motor positions are the control inputs while the elastic joint torque and the joint stiffness are the actuators output. Here we define: i) the torque and stiffness characteristics of these actuators, ii) identify the necessary and sufficient conditions that make *independent torque and stiffness modulation* viable and iii) introduce the *fundamental smoothness conditions* inherent to compliant actuated systems.

[4]This argument holds (under C.2 and/or C.3) even if no model-specific feed-forward torque is included in the control law (12) (i.e., $\hat{\boldsymbol{\tau}}_\theta \equiv \mathbf{0}$).

[5]This is because the non-linear (and possibly non-smooth) frictional terms, that are difficult to model and identify, are decoupled from the link-side dynamics by the intrinsic compliance of the actuators.

A. Torque characteristic of the actuators

According to (9), using the motor side positions $\boldsymbol{\theta}$ as inputs

$$\boldsymbol{\tau}_{E1} = \boldsymbol{\tau}_{E1}(\mathbf{q}, \boldsymbol{\theta}), \tag{16}$$

provides the *elastic joint torques* as actuator outputs[6]. The state (i.e., $\mathbf{q}$) dependence of this static torque characteristic is due to the passive elasticity, in-built in the actuators, and not due to active feedback [36]. By setting a constant motor position $\boldsymbol{\theta} = \mathbf{c}$, (16) defines the *passive torque characteristic* of the actuators, $\boldsymbol{\tau}_c(\mathbf{q}) = \boldsymbol{\tau}(\mathbf{q}, \mathbf{c})$, while by changing the motor positions, $\boldsymbol{\theta} = \boldsymbol{\theta}(t)$, these passive mechanical characteristic are *actively modulated*. In order to do this, however, the actuators should be *torque controllable*. A *necessary condition* for torque controllability is provided if the number of motor inputs is at least equal to the number of torque outputs (i.e., $m \geq n$), while a *sufficient condition* is given by

$$d = \det\left(\left[\frac{\partial \boldsymbol{\tau}}{\partial \boldsymbol{\theta}}\right]\left[\frac{\partial \boldsymbol{\tau}}{\partial \boldsymbol{\theta}}\right]^{+}\right) \neq 0. \tag{17}$$

It may be of interest to note that this condition is state dependent, and that real VS actuators may have *singular regions in their work-space* where torque controllability is not provided. While this can lead to reduced control authority, it may not adversely affect the present feed-forward scheme since we do not use the inversion of (16) in the implementation.

B. Stiffness characteristic of the actuators

By definition, stiffness relates the torque response to position perturbation. In this light, the *output stiffness of the actuators* $\mathbf{K} \in \mathbb{R}^{n\times n}$, that is, the stiffness of the actuators seen by the rigid body dynamics, is given by

$$\mathbf{K} = \mathbf{K}(\mathbf{q}, \boldsymbol{\theta}) = -\frac{\partial \boldsymbol{\tau}}{\partial \mathbf{q}}. \tag{18}$$

By analogy with the previous section, one can define the *design specific* (often highly non-linear) *passive stiffness characteristics* of the actuators by fixing the motor positions, $\mathbf{K}_c(\mathbf{q}) = \mathbf{K}(\mathbf{q}, \mathbf{c})$. On the other hand, using time-dependent motor positions, the actuator stiffness and torque can be *simultaneously* modulated, although they may not be independent. *Independent modulation of $\boldsymbol{\tau}(\mathbf{q}, \boldsymbol{\theta})$ and $\mathbf{K}(\mathbf{q}, \boldsymbol{\theta})$ through $\boldsymbol{\theta}(t)$ is, however, one of the key attributes of variable-stiffness actuators.* The *necessary* condition to achieve that is provided by actuation redundancy (i.e., $m > n$) while a *sufficient* condition is given by

$$r = \operatorname{rank}\left(\left[\frac{\partial \mathbf{k}}{\partial \boldsymbol{\theta}}\right]\left(\mathbf{I} - \left[\frac{\partial \boldsymbol{\tau}}{\partial \boldsymbol{\theta}}\right]^{+}\left[\frac{\partial \boldsymbol{\tau}}{\partial \boldsymbol{\theta}}\right]\right)\right) \neq 0, \tag{19}$$

where $\mathbf{k} = vec(\mathbf{K}) \in \mathbb{R}^{n^2}$ is the column vectorized stiffness matrix, $\mathbf{I} \in \mathbb{R}^{m\times m}$ is an identity matrix while $(*)^+$ denotes the Moore-Penrose generalized inverse of $(*)$, see [48].

Practically, (19) ensures that the motor positions that cannot affect the joint torques, can be used to modulate the joint stiffness. It is important to note that (19) is not sufficient to modulate *all components* of the stiffness matrix. Indeed, the number of components that can be independently modulated through $\boldsymbol{\theta}$ is defined by r. It is also important to recognize that the above condition is not satisfied for series elastic actuators (i.e., $m = n \Rightarrow \mathbf{I} - (\partial\boldsymbol{\tau}/\boldsymbol{\theta})^{+}(\partial\boldsymbol{\tau}/\boldsymbol{\theta}) \equiv \mathbf{0}$), while it must be satisfied, at least for some portion of the work-space, for variable stiffness actuators.

C. Fundamental smoothness conditions

When the smoothness properties of the link and the motor-side positions[7] i.e., $\boldsymbol{\theta}(t) \in \mathbb{C}^1$ and $\mathbf{q}(t) \in \mathbb{C}^2$ are reflected through the actuators[8], the output torque and stiffness characteristics admit the following continuity and smoothness conditions as functions of time:

$$\boldsymbol{\tau}(\mathbf{q}(t), \boldsymbol{\theta}(t)) \in \mathbb{C}^1 \quad \text{and} \quad \mathbf{K}(\mathbf{q}(t), \boldsymbol{\theta}(t)) \in \mathbb{C}^0. \tag{20}$$

The above two conditions may be seen as *fundamental smoothness requirements* asserted by general principle of dynamics to a *general class of compliant actuators* that admit continuously differentiable torque-angle characteristic[9] (16).

It is of interest to note here that exact link-side position and stiffness tracking on variable stiffness systems is only possible if the desired position/stiffness trajectories are at least four/two times differentiable respectively, see [32]. Compared to (20), such tracking scheme requires stronger conditions i.e., an actuator that provides a two-times continuously-differentiable stiffness-angle relationship $\mathbf{K}(\mathbf{q}, \boldsymbol{\theta})$ in addition to motor-side positions $\boldsymbol{\theta}(t) \in \mathbb{C}^2$ generated by continuous motor torques. On the other hand, torque and stiffness control may be instantaneous with respect to the time-scale relevant to the rigid body dynamics on *non-compliant actuators*. Accordingly, a similar condition to (20) *does not* restrict active impedance control on robots driven with (torque controllable) non-compliant actuators [36].

V. Actuation Constraints

Conditions (17) and (19) may be seen as design constraints while (20) provides fundamental physical constraints. There are, however, additional constraints that also restrict the output torque and stiffness of compliant actuators. In the following, we introduce these *actuation constraints*.

A. Constraints on the motor trajectories

Regardless of whether the system is compliantly actuated or not, the motor trajectories are subject to inequality constraints

[6]For notational convenience we drop the index in the above equation, such that $\boldsymbol{\tau} = \boldsymbol{\tau}_{E1}$ will denote the elastic joint torques in the remainder of this paper.

[7]$\mathbb{C}^s$ denotes the set of all s-times differentiable functions.

[8]Here we assume that the motor positions may be generated by piecewise-continuous motor torques that leads to continuously differentiable motor-positions. This assumption asserts that the dynamics in the electrical domain associated with the motor-torque control is negligible on the time scale relevant in mechanical domain. This assumption is accepted here since it leads to the weakest continuity requirement that is physically justified in the present investigation.

[9]While it is possible, in principle, to design actuators that have non-differentiable torque-angle characteristic (in which case the stiffness $\mathbf{K} = -\partial\boldsymbol{\tau}/\partial\mathbf{q}$ may not be well defined) such designs are currently not employed in practical applications and, as such, are not considered here.

due to *range*, *rate* and *acceleration* limits posed by their servo-controlled dynamics. The admissible set of trajectories subject to these constraints can be defined by

$$\Theta = \{\boldsymbol{\theta} \in \mathbb{C}^1([0,T],\mathbb{R}^m) : \boldsymbol{\theta}_m \preceq \boldsymbol{\theta}(t) \preceq \boldsymbol{\theta}_M, \\ |\dot{\boldsymbol{\theta}}(t)| \preceq \dot{\boldsymbol{\theta}}_M, |\ddot{\boldsymbol{\theta}}(t)| \preceq \ddot{\boldsymbol{\theta}}_M\}, \tag{21}$$

where $\boldsymbol{\theta}_m$ and $\boldsymbol{\theta}_M$, ($\boldsymbol{\theta}_m \prec \boldsymbol{\theta}_M$) denote the lower and the upper bounds on the motor positions while $\dot{\boldsymbol{\theta}}_M$ and $\ddot{\boldsymbol{\theta}}_M$ ($\mathbf{0} \prec \dot{\boldsymbol{\theta}}_M$, $\mathbf{0} \prec \ddot{\boldsymbol{\theta}}_M$) are the achievable maximal velocities and accelerations respectively. To be physically realizable, the motor trajectories should adhere to these limitations: $\boldsymbol{\theta}(t) \in \Theta$.

B. Deformation limits on the compliant elements

In addition to the constraints above, series elastic actuators and variable stiffness devices may also posses *non-linear state inequality constraints*, due to limits on the deformation of the compliant elements. The admissible set of the actuator positions, associated with these constraints is formally defined by

$$\Phi = \{\boldsymbol{\phi} \in \mathbb{C}^1(\mathbb{R}^n \times \mathbb{R}^m, \mathbb{R}^m) : \\ \boldsymbol{\phi}_m(\boldsymbol{\theta}) \preceq \boldsymbol{\phi}(\mathbf{q},\boldsymbol{\theta}) \preceq \boldsymbol{\phi}_M(\boldsymbol{\theta})\}, \tag{22}$$

where $\boldsymbol{\phi}$ denotes the quantities (e.g., length of the springs, see Fig.2) to be constrained during the motion, while $\boldsymbol{\phi}_m$ and $\boldsymbol{\phi}_M$ ($\boldsymbol{\phi}_m \prec \boldsymbol{\phi}_M$) define, the possibly state-dependent, lower and upper bounds.

It is noteworthy that violation of these constraints would not only lead to behavior that considerably differ from the planned one, but it would *permanently damage the actuators*[10]. Accordingly, enforcing the above constraints, $\boldsymbol{\phi}(\mathbf{q},\boldsymbol{\theta}) \in \Phi$ may often be prioritized in *real-world applications*.

VI. Optimization under actuation constraints

Here we present an *optimal control formulation* and an approach to *trajectory optimization* to plan control strategies best suited to the dynamics and the specificity of the task considered. Using this approach we can systematically treat the complexity (i.e., non-linearity, redundancy and constraint) inherent to compliantly actuated robots. While finding control programs i.e., *desired motor trajectories* (and the associated torque and passive impedance) under actuation constraints poses significant challenges, the present formulation is able to deal with this in a systematic way, without problem specific derivation or difficult computation.

In the following, we: i) derive a minimalistic (physically consistent) model for compliantly actuated robots, ii) introduce the treatment of constraints, iii) propose an optimal control formulation and finally iv) define the optimal motor program for hardware implementations.

[10]In this case, the moving elements in the actuators would run into hard stops and/or the compliant element (spring) would be operated in the plastic region, and as such permanently deformed.

A. A minimalistic model for optimization

In this section, we assume that conditions C.2 and C.3, stated in Section III-A, apply. Consistent with the former condition is Spong's assumption by which

A.3 the rotational kinetic energy of each motor-gearbox assembly is due approximately to the self-rotation i.e., $\mathcal{T}_{12} \approx 0$ in (1), see [19].

Under A.3 the following simplifications apply (please see (1) and (5)-(7)):

$$\mathbf{S} \approx \mathbf{0}, \mathbf{C} = \mathbf{C}(\mathbf{q},\dot{\mathbf{q}}), \mathbf{C}_q \approx \mathbf{0}, \mathbf{C}_\theta \approx \mathbf{0}. \tag{23}$$

As a consequence, the original equation (4) supplemented with the control law (12) reduces to

$$\mathbf{M}(\mathbf{q})\ddot{\mathbf{q}} + \mathbf{C}(\mathbf{q},\dot{\mathbf{q}})\dot{\mathbf{q}} + \mathbf{D}\dot{\mathbf{q}} + \mathbf{G}(\mathbf{q}) = \boldsymbol{\tau}(\mathbf{q},\boldsymbol{\theta}), \tag{24}$$

$$\ddot{\boldsymbol{\theta}} + 2\boldsymbol{\kappa}\dot{\boldsymbol{\theta}} + \boldsymbol{\kappa}^2\boldsymbol{\theta} = \boldsymbol{\kappa}^2\boldsymbol{\theta}_d, \tag{25}$$

where (25) resembles a critically-damped[11] closed-loop motor dynamics (15) where $\boldsymbol{\beta} = \boldsymbol{\kappa}$, see Section III-A. We note that if the gear reduction is not particularly high (i.e., A.3 does not apply) one should complement the link-side dynamics (24) with additional inertial terms indicated by (4). On the other hand, the validity of (25) is not conditioned on highly geared actuation as long as high-gain servo-control is employed (please see Section III). The purpose of this latter equation is to plan for realizable (smooth enough) motor trajectories i.e., $\boldsymbol{\theta}$ that are consistent with the constraints. In the present paper, we consider (24) and (25) to be a *minimalistic representation* of (4)-(10) which ensures the fundamental continuity conditions (20) for any, at least, piecewise-continuous desired trajectory $\boldsymbol{\theta}_d$.

B. Treatment of constraints

While incorporating the constraints (21) and (22), into the optimization is vital, numerical treatment of them is non-trivial. Indeed, solving an optimal control problem with *state inequality constraints* is often computationally demanding and complicates the numerical treatment (see Section IX). Moreover, excessive application of constraints makes the associated formulation more susceptible to local-minima issues. Finding an optimal solution to such a formulation is known to be difficult. Therefore, reduction of the number and complexity of the constraints is often preferred in practice. Here we address this issue by replacing *non-linear state inequality constraints* with *canonical control constraints* that are easier to treat numerically. To achieve this, we present a differential-algebraic transformation that enables us to *explicitly embed number of inequality constraints as hard constraints* (i.e., constraints that cannot be violated) into the dynamics.

[11]It may be important to note here that assuming critical-damped closed-loop motor dynamics is not restrictive. This is partly because critically-damping is often preferred in trajectory tracking schemes (especially for systems driven be compliant actuators), but also because the subsequent results, that depend on this assumption, can be generalized to over-damped systems (i.e., $\boldsymbol{\beta} \succ \boldsymbol{\kappa}$).

1) Transforming the constraints: Let us now consider a set of user defined non-linear inequalities

$$\Psi = \{\boldsymbol{\psi} \in \mathbb{C}^1(\mathbb{R}^n \times \mathbb{R}^m, \mathbb{R}^m) : \boldsymbol{\psi}_m(\boldsymbol{\theta}) \preceq \boldsymbol{\psi}(\mathbf{q}, \boldsymbol{\theta}) \preceq \boldsymbol{\psi}_M(\boldsymbol{\theta})\}, \quad (26)$$

where Ψ denotes the admissible set of quantities $\boldsymbol{\psi} \in \mathbb{R}^m$ (e.g., including motor positions $\boldsymbol{\theta}$ and/or spring lengths $\boldsymbol{\phi}$) to be constrained during the motion while $\boldsymbol{\psi}_m \prec \boldsymbol{\psi}_M$ are the associated (possibly state-dependent) lower and upper bounds. We assume that these bounds are also continuously differentiable functions of their arguments.

In a special case when $\boldsymbol{\psi} = \boldsymbol{\theta}$, (26) reduces to the range constraints on the motor positions while in the another extreme case when $\boldsymbol{\psi} = \boldsymbol{\phi}(\mathbf{q}, \boldsymbol{\theta})$, (26) would reduce to (22). To embed these constraints into the dynamics, we may proceed in the following way:

- first define a *canonical input set*[12]

$$Z_d = \{\mathbf{z}_d \in PC([0, T], \mathbb{R}^m) : \mathbf{0} \preceq \mathbf{z}_d \preceq \mathbf{1}\}, \quad (27)$$

- then introduce a set of *canonical state variables*

$$z_i = \frac{\psi_i - \psi_{im}}{\psi_{iM} - \psi_{im}}, \quad (28)$$

- and finally generate $\mathbf{z} = [z_1, z_2, ..., z_m]^T$ through a *second-order critically-damped differential equation*

$$\ddot{\mathbf{z}} + 2\boldsymbol{\alpha}\dot{\mathbf{z}} + \boldsymbol{\alpha}^2\mathbf{z} = \boldsymbol{\alpha}^2\mathbf{z}_d, \quad (29)$$

where $\forall i \in \{1, 2, ..., m\}$, $\alpha_i > 0$, $\boldsymbol{\alpha}^2 = \mathrm{diag}\{\alpha_i^2\}$ and $z_i(0) \in [0, 1]$ is defined by (28) based on the initial state of the system.

This *differential-algebraic transformation*, (28) and (29), provides constraint consistent state output for any admissible control input

$$\forall \mathbf{z}_d \in Z_d \Rightarrow \boldsymbol{\psi} \in \Psi. \quad (30)$$

It may be of interest to recognize that this transformation is not problem specific, but its application requires one parameter $\boldsymbol{\alpha}$ to be set for every embedded constraint; this is detailed in Sections VI-C1 and VI-C2.

2) Computing the motor trajectories: One of the main question regarding the proposed transformation is how to include the new state variables $\mathbf{z}$ into the dynamics (24) and (25). To this end, we consider (28) to be a *coordinate transformation* that relates $\mathbf{z}$ with $\boldsymbol{\theta}$ and $\mathbf{q}$ through the following relation

$$\boldsymbol{\Psi}(\mathbf{q}, \boldsymbol{\theta}, \mathbf{z}) = \mathbf{0}, \quad (31)$$

where $\boldsymbol{\Psi}(\mathbf{q}, \boldsymbol{\theta}, \mathbf{z}) := \boldsymbol{\psi}(\mathbf{q}, \boldsymbol{\theta}) - \mathrm{diag}(\boldsymbol{\psi}_M(\boldsymbol{\theta}) - \boldsymbol{\psi}_m(\boldsymbol{\theta}))\mathbf{z} - \boldsymbol{\psi}_m(\boldsymbol{\theta})$. Using (31), we may find the motor trajectories $\boldsymbol{\theta}$ as functions of the canonical states $\mathbf{z}$ (and $\mathbf{q}$). Indeed, according to the implicit function theorem [49], one can (at least locally) define the following inverse mapping of (31)

$$\boldsymbol{\theta} = \boldsymbol{\Psi}_\theta^{-1}(\mathbf{q}, \mathbf{z}), \quad (32)$$

for every $(\mathbf{q}, \mathbf{z})$ for which $\partial\boldsymbol{\Psi}/\partial\boldsymbol{\theta} \in \mathbb{R}^{m \times m}$ is a full-rank matrix. i.e.,

$$\det(\partial\boldsymbol{\Psi}/\partial\boldsymbol{\theta}) \neq 0. \quad (33)$$

[12] $PC([0, T], \mathbb{R}^m)$ denotes a set of piecewise continuous functions mapping $[0, T]$ to $\mathbb{R}^m$.

In addition, as long as $\boldsymbol{\psi}$, $\boldsymbol{\psi}_m$ and $\boldsymbol{\psi}_M$ are continuously differentiable with respect to their arguments (as assumed), the same is true for the inverse mapping $\boldsymbol{\Psi}_\theta^{-1}(\mathbf{q}, \mathbf{z})$ and the motor trajectories $\boldsymbol{\theta}$ computed using (32).

It is important to note that fulfillment of (33) depends on the constraints. In particular, if (26) represents the constraints on the motor trajectories, the inverse mapping $\boldsymbol{\Psi}_\theta^{-1}$ exist unconditionally (this is the case for the model of the 2-link arm driven by *mechanically adjustable compliance and controllable equilibrium position actuators* (MACCEPAs) used in Section VII-B, see also Section VI-C1). It is also important to point out that the proposed scheme favors constraints that admit an analytical representation of $\boldsymbol{\Psi}_\theta^{-1}$ and as such explicit computation of the motor trajectories (as in the model of the DLR Hand-Arm System used in Section VII-C, see also Section VI-C2). When this is not possible, one may employ Newton's method [50] to solve (31) for $\boldsymbol{\theta}$ directly. As long as the inverse mapping is well defined, i.e., (33) holds, the associated iterative computation can be well initialized and reliably solved with little computational effort[13].

Finally, we note that the *number* of state inequality constraints that can be treated in this way is defined by the number of control inputs (motor positions) m. In the case when only the motor position are constrained, this allows full embedding of the constraints (discussed in Section VI-C1). In the case when deformation limits are also present, the proposed embedding can be used to *reduce the number of constraints* to be treated by a complementary approach. We note that in such a case, the proposed embedding may be employed on the complex deformation limits (22) that are vital to be enforced, while leaving the simpler motor position constraints to be treated separately (as exemplified in Section VII-C).

C. State-space representation

Let us now formally introduce the *state vector* and the *control inputs* as:

$$\mathbf{x} = \begin{bmatrix} \mathbf{x}_1 \\ \mathbf{x}_2 \\ \mathbf{x}_3 \\ \mathbf{x}_4 \end{bmatrix} = \begin{bmatrix} \mathbf{q} \\ \dot{\mathbf{q}} \\ \mathbf{z} \\ \dot{\mathbf{z}} \end{bmatrix}, \quad \mathbf{u} = \mathbf{z}_d, \quad (34)$$

where $\mathbf{x} \in \mathbb{R}^{2(n+m)}$ and $\mathbf{u}$ belongs to a canonical box-constrained set

$$U = \{\mathbf{u} \in PC([0, T], \mathbb{R}^m) : \mathbf{0} \preceq \mathbf{u} \preceq \mathbf{1}\}. \quad (35)$$

Using this notion, the state-space representation of the original constrained system (24)–(26) becomes

$$\dot{\mathbf{x}} = \mathbf{f}(\mathbf{x}, \mathbf{u}), \quad (36)$$

$$\mathbf{f} = \begin{bmatrix} \mathbf{x}_2 \\ -\mathbf{M}^{-1}(\mathbf{x}_1)(\mathbf{C}(\mathbf{x}_1, \mathbf{x}_2)\mathbf{x}_2 + \mathbf{D}\mathbf{x}_2 + \mathbf{G}(\mathbf{x}_1) - \mathbf{T}(\mathbf{x}_1, \mathbf{x}_3)) \\ \mathbf{x}_3 \\ -2\boldsymbol{\alpha}\mathbf{x}_4 - \boldsymbol{\alpha}^2\mathbf{x}_3 + \boldsymbol{\alpha}^2\mathbf{u} \end{bmatrix},$$

[13] This is because one can effectively initialize Newton's method for the computation of the motor positions $\boldsymbol{\theta}(t_{n+1})$ using the *nearby* solution for the previous time step $\boldsymbol{\theta}(t_n)$, since $\boldsymbol{\theta} = \boldsymbol{\theta}(t)$ defined by (32) is a continuously-differentiable function.

where $\mathbf{T} = \mathbf{T}(\mathbf{x}_1, \mathbf{x}_3)$ denotes the actuator torques expressed through the new state variables

$$\mathbf{T} = \mathbf{T}(\mathbf{x}_1, \mathbf{x}_3) = \mathbf{T}(\mathbf{q}, \mathbf{z}) = \boldsymbol{\tau}(\mathbf{q}, \boldsymbol{\Psi}_\theta^{-1}(\mathbf{q}, \mathbf{z})). \tag{37}$$

Taking these together, the proposed formulation is fully specified with (36), (37) where the control inputs are restricted with the simplest set of inequality constraints (i.e., canonical box-constraints) (35), but it *does not involve any state inequality constraints* e.g., (26).

In order to employ this formulation, however, one must define one parameter for every embedded constraint $\boldsymbol{\alpha} = \mathrm{diag}\{\alpha_i\}$. If these parameters are positive, $\forall \alpha_i > 0$, then the range constraints (26) cannot be violated[14]. In the following, we give a *physical interpretation* of $\boldsymbol{\alpha}$ and discuss how to select this parameter in two important practical cases of interest.

1) Embedding bandwidth limitations on the motor dynamics: Let us now assume that, for a given actuator, there are no complex state inequality constraints (e.g., there are no limitations on the elastic deformation of the springs), or even if such limits exist, they are not expected to be violated during the motion[15]. In that case, any admissible motor trajectory must obey the range, rate and acceleration limits given by (21):

$$\boldsymbol{\theta} \in \Theta. \tag{38}$$

Using the formulation in the previous section we can enforce the associated range limits $\boldsymbol{\theta}_m \preceq \boldsymbol{\theta} \preceq \boldsymbol{\theta}_M$, by setting:

i) $\boldsymbol{\psi} = \boldsymbol{\theta}$, $\boldsymbol{\psi}_m = \boldsymbol{\theta}_m$, $\boldsymbol{\psi}_M = \boldsymbol{\theta}_M$.

In this case, the inverse mapping (32) can be explicitly defined

$$\boldsymbol{\theta} = \boldsymbol{\Psi}_\theta^{-1}(\mathbf{z}) = \mathrm{diag}(\boldsymbol{\theta}_M - \boldsymbol{\theta}_m)\mathbf{z} + \boldsymbol{\theta}_m. \tag{39}$$

Direct implication of this relation is that, for a critically damped motor dynamics, $\boldsymbol{\alpha}$ coincides with the position gains $\boldsymbol{\kappa}$ in (25). Accordingly, we can ensure that not only the range constraints but also the bandwidth limits associated with the rate and acceleration constraints $|\dot{\boldsymbol{\theta}}| \preceq \dot{\boldsymbol{\theta}}_M$ and $|\ddot{\boldsymbol{\theta}}| \preceq \ddot{\boldsymbol{\theta}}_M$ are satisfied by choosing:

ii) $\alpha_i \in (0, \alpha_{iM}]$, $\forall i \in \{1, 2, ..., m\}$ where

$$\alpha_{iM} = e \times \min\left\{ \frac{\dot{\theta}_{iM}}{\theta_{iM} - \theta_{im}}, \sqrt{\frac{\ddot{\theta}_{iM}}{\theta_{iM} - \theta_{im}}} \right\}. \tag{40}$$

Note that embedding the velocity and acceleration limits is indeed possible in this way since $\boldsymbol{\alpha}_M$ represents the maximal position gains that guarantee (21), under piecewise-continuous inputs $\mathbf{u} \in U$. Regarding the choice of α_i, we note that any $\alpha_i \in (0, \alpha_{iM}]$ would ensure (21), however, $\alpha_i = \alpha_{iM}$ would lead to the *best exploitation of the motor-side dynamics* and as such it may be preferred in practice[16]. It is noteworthy that under the two conditions (i) and (ii) introduced in this section, the formulation (34)–(37) reduces to the one proposed in [18]. For further application of this formulation, the reader is referred to [41].

2) Embedding deformation limits on the elastic elements: Let us now consider another case when the length of the springs in the actuators have to be constrained during the motion. In this case, we may require:

$$\boldsymbol{\phi}(\mathbf{q}, \boldsymbol{\theta}) \in \Phi. \tag{41}$$

Using the proposed formulation (35)–(37), the above restriction can be ensured by setting: $\boldsymbol{\psi} = \boldsymbol{\phi}(\mathbf{q}, \boldsymbol{\theta})$. In that case, the canonical states $\mathbf{z}$ represent the normalized spring lengths

$$\boldsymbol{\phi}(\mathbf{q}, \boldsymbol{\theta}) = \mathrm{diag}(\boldsymbol{\phi}_M(\boldsymbol{\theta}) - \boldsymbol{\phi}_m(\boldsymbol{\theta}))\mathbf{z} + \boldsymbol{\phi}_m(\boldsymbol{\theta}). \tag{42}$$

The inverse mapping $\boldsymbol{\theta} = \boldsymbol{\Psi}_\theta^{-1}(\mathbf{q}, \mathbf{z})$, that solves this relation for $\boldsymbol{\theta}$, is in general link-side position dependent and may be hard to define explicitly. A notable exception to this is when the spring length is a linear function of a motor-side position: e.g., $\phi_i = \theta_i - q_i$ as in elastic joint robots or in the model of the DLR Hand-Arm System, see Section VII-C. In such cases, the motor positions can be explicitly defined: $\theta_i = \psi_\theta^{-1}(q_i, z_i) = q_i + (\phi_{iM} - \phi_{im})z_i + \phi_{im}$ (as long as ϕ_{iM} and ϕ_{im} do not depend on θ_i).

Regardless of whether one can explicitly compute the motor trajectories, the dynamics associated with $\mathbf{z}$ (third and fourth lines in (36)) defines the dynamics of the normalized spring motion. The physical implication of this is that, here $\boldsymbol{\alpha}$ limits the bandwidth of the entire system (i.e., link-side and motor-side dynamics), and as such it cannot be used to embed the bandwidth limitations on the actuators alone. In this light, the velocity and acceleration limits $|\dot{\boldsymbol{\theta}}| \preceq \dot{\boldsymbol{\theta}}_M$ and $|\ddot{\boldsymbol{\theta}}| \preceq \ddot{\boldsymbol{\theta}}_M$ cannot be embedded into the formulation, in a way described in the previous section, and as such remain to be treated by a complementary approach. In Section VII-C we illustrate this through simulations and a practical application.

D. The optimal control problem

In order to define optimal control strategies for compliantly actuated robots, we consider the following control problem: *For a given finite time interval $t \in [0, T]$, and for a given initial state of the system $\mathbf{x}(0) = \mathbf{x}_0$, find the control inputs $\mathbf{u}$ that minimize the optimization criterion defined by*

$$J = h(T, \mathbf{x}(T)) + \int_0^T c(t, \mathbf{x}(t), \mathbf{u}(t))dt, \tag{43}$$

where $J \in \mathbb{R}$ is the cost functional, $h(T, \mathbf{x}(T)) \in \mathbb{R}$ is the terminal cost, while $c(t, \mathbf{x}, \mathbf{u}) \in \mathbb{R}$ is the running cost used to encode the control objectives into the formulation [52]. This minimization problem is restricted with the plant dynamics

$$\dot{\mathbf{x}} = \mathbf{f}(\mathbf{x}, \mathbf{u}), \tag{44}$$

and the control constraints (i.e., canonical box-constraints)

$$\mathbf{u} \in U, \tag{45}$$

defined by (35)–(37).

[14]This follows directly from $\mathbf{u} \in U \Rightarrow \mathbf{0} \preceq \mathbf{x}_3 = \mathbf{z} \preceq \mathbf{1}$ and (28).

[15]This assumption may be ensured through design as is done for our 2-link variable stiffness robot introduced in Section VII-B.

[16]It is also noteworthy that α_{iM} computed from (40) often turns out to be conservative. There are two main reasons to this. One is because α_{iM} is calculated assuming a maximal step response command $\theta_{iM} - \theta_{im}$ although this may not be the usual command in practice, while the another is because real servo-systems are often deliberately pushed to saturation to improve their tracking performance compared to an unsaturated ideal linear servo model [51]. Due to these reason one may chose $\alpha_i > \alpha_{iM}$ as long as this does not jeopardize the tracking accuracy.

In this paper we employ the iLQR framework [53] in order to find the optimal solutions $\mathbf{x}^* = \mathbf{x}^*(t)$ and $\mathbf{u}^* = \mathbf{u}^*(t)$ for the *constrained optimal control problem* defined by (43)–(45). A discussion on alternative methods to solve this problem is provided in the Appendix. In the following, we show how to compute the desired motor trajectories required in practical implementations, once the optimal state trajectories are found.

E. Computing the desired motor trajectories

If the constraints on the actuators (21) are incorporated into the formulation, the motor trajectories computed by (32), i.e., $\boldsymbol{\theta}^* = \boldsymbol{\Psi}_\theta^{-1}(\mathbf{q}^*(t), \mathbf{z}^*(t)) = \boldsymbol{\Psi}_\theta^{-1}(\mathbf{x}_1^*(t), \mathbf{x}_3^*(t))$, will be within the bandwidth of the actuators. This means that by using servo-control on the motor-side, see (15) [or (25)], with optimal desired trajectories computed by

$$\boldsymbol{\theta}_d = \boldsymbol{\Psi}_\theta^{-1}(\mathbf{q}^*(t), \mathbf{z}^*(t)) = \boldsymbol{\Psi}_\theta^{-1}(\mathbf{x}_1^*(t), \mathbf{x}_3^*(t)), \tag{46}$$

will ensure that the real motor positions $\boldsymbol{\theta}$ closely follow the corresponding optimal motion $\boldsymbol{\theta}^*$, i.e.,

$$\boldsymbol{\theta} \approx \boldsymbol{\theta}_d = \boldsymbol{\theta}^*. \tag{47}$$

It is noteworthy that this argument does not rest on the linearity of the closed-loop controlled motor dynamics. As such it remains valid even if the servo-system is deliberately pushed into saturation to provide better tracking performance [51].

VII. Application

In this section, we provide numerical simulations and hardware experiments to demonstrate the viability of the proposed optimal control formulation. These simulations and experiments involve two *redundantly actuated* variable stiffness robots, specifically:

- the two-link robot [18], shown in Fig.3a, driven by MACCEPAs [54] (see Fig.3b,c) and
- the integrated DLR Hand-Arm System (HASy) [1], shown in Fig.7, equipped with variable stiffness floating spring joints (FSJ) [7] (see Fig.5a,b).

The purpose of the presented numerical study is to illustrate the effect of the actuation constraints on robotic systems driven by series elastic and/or variable stiffness actuators. The purpose of the hardware experiments is to demonstrate the viability of the constraint embedding method and the proposed optimal impedance control planning under real-world conditions.

A. Control task

The following investigation involves a ball throwing task. This task is associated with fast movements where exploitation of the full capacity of the actuators, under given constraints, is important to improve task performance (i.e., distance thrown). Within the framework of optimal control, ball-throwing is represented with the following objective functional (please see [18]):

$$J_t = -d + \frac{1}{2}\int_0^T (w\|\mathbf{F}\|^2 + \epsilon\|\mathbf{u}\|^2)dt, \tag{48}$$

where T is the time permitted to task execution, $d = d(\mathbf{q}(T), \dot{\mathbf{q}}(T))$ is the distance thrown, $\mathbf{F} = \mathbf{F}(\mathbf{q}, \boldsymbol{\theta})$ is the spring force, $\mathbf{u}$ is the control input while $\| * \|$ denotes the Euclidean norm.

Here, we consider a predominantly distance maximization task characterized with small effort penalization (i.e., $w \to 0$), and a small regularization term (i.e., $0 < \epsilon \ll 1$) that makes the objective explicitly control-dependent and the control problem non-singular. It is important to note that *the optimal strategy should adhere to the actuation constraints* (21) and (22), since it will only be physically realizable if these constraints are satisfied.

B. Two-link variable stiffness robot

The variable stiffness robot, shown in Fig.3, has two kinematic degrees of freedom (DOFs) and is equipped with two variable stiffness actuators (VSAs) driven with four motors. The configuration of this system is defined with the corresponding joint angles $\mathbf{q} = [q_1, q_2]^T$ and motor angles $\boldsymbol{\theta} = [\theta_1, \theta_2, \theta_3, \theta_4]^T$. One of the motors in each VSAs (θ_1 and θ_2) changes the joint equilibrium, while the another (θ_3 and θ_4) modulates the passive joint stiffness. In Figs.3c-e we show the actuation mechanism, and the torque-angle and torque-stiffness characteristics of these actuators.

1) Simulation and experimental results: In Fig. 4a and Fig. 4b we show the effect of the actuators range and rate (bandwidth) limitation on the optimal control strategy. It can be recognized that using larger stiffness range $\theta_{3,4} \in [0, \pi/2]\text{rad}$ and fast (high-bandwidth) actuators for stiffness modulation $\alpha_{3,4} = 5[\sqrt{10}, \sqrt{10}]\text{s}^{-1}$, instead of small ranges $\theta_{3,4} \in [0, \pi/4]\text{rad}$ and slow (low-bandwidth) actuators $\alpha_{3,4} = 5[1, 1]\text{s}^{-1}$, not only *affects the systems performance*, but it can also *qualitatively modify* the stiffness control strategy. Specifically, when the actuators are slow, active modulation of the torque-stiffness characteristics of the joints appear not to be beneficial (see gray lines in Fig. 4a2,b2), as opposed to the case when the same task is realized with actuators capable of fast stiffness modulation (see black lines in Fig. 4a2,b2). Moreover, when the stiffness range is smaller, the difference between variable and constant stiffness control becomes less apparent. *These results illustrate the crucial effects of various actuation constraint on optimal (impedance/stiffness) control strategies and support our claim by which these constraints are vital to be considered during control planning.*

2) Discussion: It is clear that having a *limited stiffness range*, the benefit provided by variable stiffness optimization compared to constant stiffness control may be negligible (e.g., see (26) in [39]). It is however less obvious that the limitation on the *speed of the stiffness modulation* can significantly impact the effect of variable stiffness control in *dynamic tasks*. At the extreme, optimal stiffness control may predict that active stiffness modulation is *not* beneficial if the speed of this modulation is slow compared to the dynamics of the movement [18]. This is to say that the optimal strategy is not only *task-specific* (i.e., that relates to the objective functional), or specific to the rigid body dynamics (that relates to the first equation in (4) [or (24)]), but it can significantly depend on the actuator

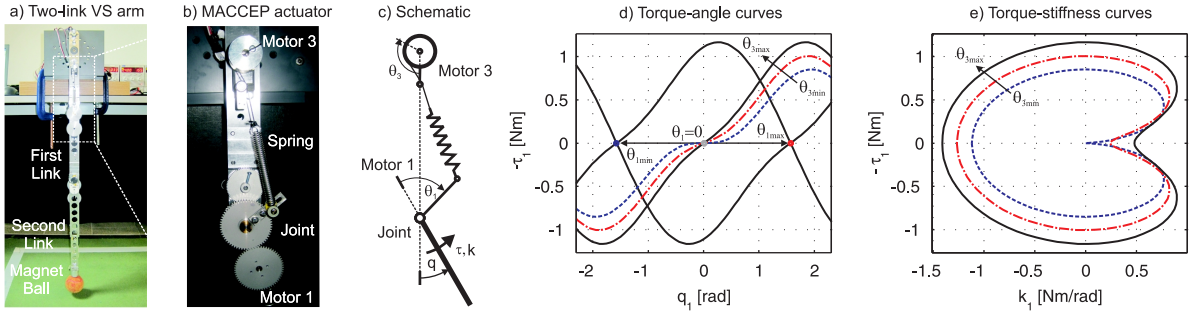

Fig. 3. a) Two-link variable-stiffness robot. b,c) Variable-stiffness actuator. The physical parameters of this system are given in [18]. d) Torque-angle curves. e) Torque-stiffness curves. Each of these curves define the passive torque-stiffness characteristic of the joint corresponding to constant stiffness commands $\theta_3 = c$ (see Sections IV-A and IV-B). By changing the equilibrium point $\theta_1 = \theta_1(t)$, but keeping the pretension commands fixed $\theta_3 = c$, one can move along these passive iso-curves in the torque-stiffness plane. However by changing the pretensioning continuously in time $\theta_3 = \theta_3(t)$, one can also modify these curves during the movement. This ability to actively modify the passive torque-stiffness characteristics of the joint allows simultaneous torque and stiffness modulation. Note that by keeping $\theta_3 = c$, this VSA becomes a series elastic actuator that has: i) non-linear torque-angle characteristic and ii) fixed torque-stiffness characteristic regardless of $\theta_1 = \theta_1(t)$. This means that under $\theta_3 = c$, this actuator cannot provide independent torque and stiffness modulation. This can be easily verified using (19). On the other hand, by fixing $\theta_1 = c$, but changing $\theta_3 = \theta_3(t)$, the actuator can generate different torque-stiffness characteristics, but it may not be able to generate any output torque e.g., if $\theta_1 = q_1$. This may be verified using (17).

dynamics (second equation in (4) [or (25)]) and the actuation constraints i.e., (21) and (22). Due to this reason, there is an obvious danger that the actuator dynamics (when slow) filters out a stiffness modulation that may be intuitively expected for a given task, but also that some *actuator-specific* stiffness control feature are mistakenly attributed as task induced.

There are important implications of this to i) new *compliant actuator designs* and also ii) interpretations concerning *human impedance control*. Regarding actuator designs, it becomes apparent that not only the range but also the dynamics (i.e., bandwidth) related to stiffness modulation needs to be part of the design specification. This is especially important for dynamic tasks, where stiffness modulation must be fast enough to become relevant on the time scale set by the task and the link-side dynamics. If this condition is not met, the benefit that may come from simultaneous torque and impedance modulation will be lost. Accordingly, just because a variable impedance actuator is capable of torque and impedance modulation, it does not mean that this feature will be beneficial. This could be due to the task itself, characteristic of the link-side dynamics, but also due to the constraints imposed by the actuators. We note that while high-bandwidth actuation may not be vital in static tasks [55], it becomes important and highly relevant in dynamic tasks. This should be taken into account when interpreting human stiffness (impedance) control strategies that is subject to realistic biological (e.g. muscle-tendon) bandwidth-limitations [56]. Regarding this last point, we note that care should also be taken when transferring experimental observations from humans to robots or vice versa [57]. *This is because impedance strategies by humans, are subject to inherent bandwidth limitations of the muscle-tendon system and as such, may not contain important task-specific features that could be utilized by robots equipped with fast actuators. This is to say that biological control strategies could be very different from those optimal for robots (even if both are obtained through optimization of the same objective functional).*

C. The DLR Hand-Arm System

The DLR-HASy is a state-of-the-art variable stiffness robot resembling the complexity of a human upper limb (see Fig.7). For the purpose of the present investigation, the simulation/experimental results conducted with this device, are reported in the sagittal plane, namely the shoulder and elbow rotation joint (i.e., $\mathbf{q} = [q_1, q_2]^T$). Both of these joints incorporate variable stiffness actuators (Fig.5a). These VSAs involve a main motor (θ_1 and θ_2) that modulate the set-point of the virtual spring and a small motor (θ_3 and θ_4) that adjust the joint stiffness, see Fig.5b. In Figs.5c-e, we show the: c) deformation limits on these actuators, d) torque-angle characteristics and e) torque-stiffness characteristics of the joints respectively.

The range/rate constraints associated with the limitations on the position and velocities of the stiffness adjuster motors $\boldsymbol{\sigma} = [\theta_3, \theta_4]^T$ and the deformation limits on the floating springs are given as:

$$\mathbf{0} \preceq \boldsymbol{\sigma} \preceq \boldsymbol{\sigma}_M, |\dot{\boldsymbol{\sigma}}| \preceq \dot{\boldsymbol{\sigma}}_M, \tag{49}$$

$$\boldsymbol{\phi}_m(\boldsymbol{\sigma}) \preceq \boldsymbol{\phi} \preceq \boldsymbol{\phi}_M(\boldsymbol{\sigma}), \tag{50}$$

where the maximal limits are defined by: $\boldsymbol{\sigma}_M = 0.178[1,1]^T\text{rad}$, $\dot{\boldsymbol{\sigma}}_M = 0.541[1,1]^T\text{rad/s}$ and $\boldsymbol{\phi}_m(\boldsymbol{\sigma}) = [\phi_{m1}(\theta_3), \phi_{m2}(\theta_4)]^T$ and $\boldsymbol{\phi}_M(\boldsymbol{\sigma}) = [\phi_{M1}(\theta_3), \phi_{M2}(\theta_4)]^T$ are the state dependent constraint boundaries depicted in Fig. 5c (dashed red lines). The present formulation encodes these as hard constraints. Additional limits to be considered are the range/rate limits associated with the main motors (i.e., that modulate the set-point of the virtual joint springs $\theta_{1,2}$, see Fig. 5d). These constraints: $\theta_{1,2m} \leq \theta_{1,2} \leq \theta_{1,2M}, |\dot{\theta}_{1,2}| \leq \dot{\theta}_{1,2M}$, where $\theta_{1,2m} = [-1.05, -0.44]^T\text{rad}$, $\theta_{1,2M} = [3.05, 2.27]^T\text{rad}$ and $\dot{\theta}_{1,2M} = 8[1,1]^T\text{rad/s}$ define the maximal ranges, are treated as soft-constraints and embedded through penalty terms in the objective functional. This is *one way* to deal with constraint that cannot be embedded into the dynamics using the present formulation.

1) Simulation: A typical simulation result is shown in Fig. 6a corresponding to high bandwidth stiffness modula-

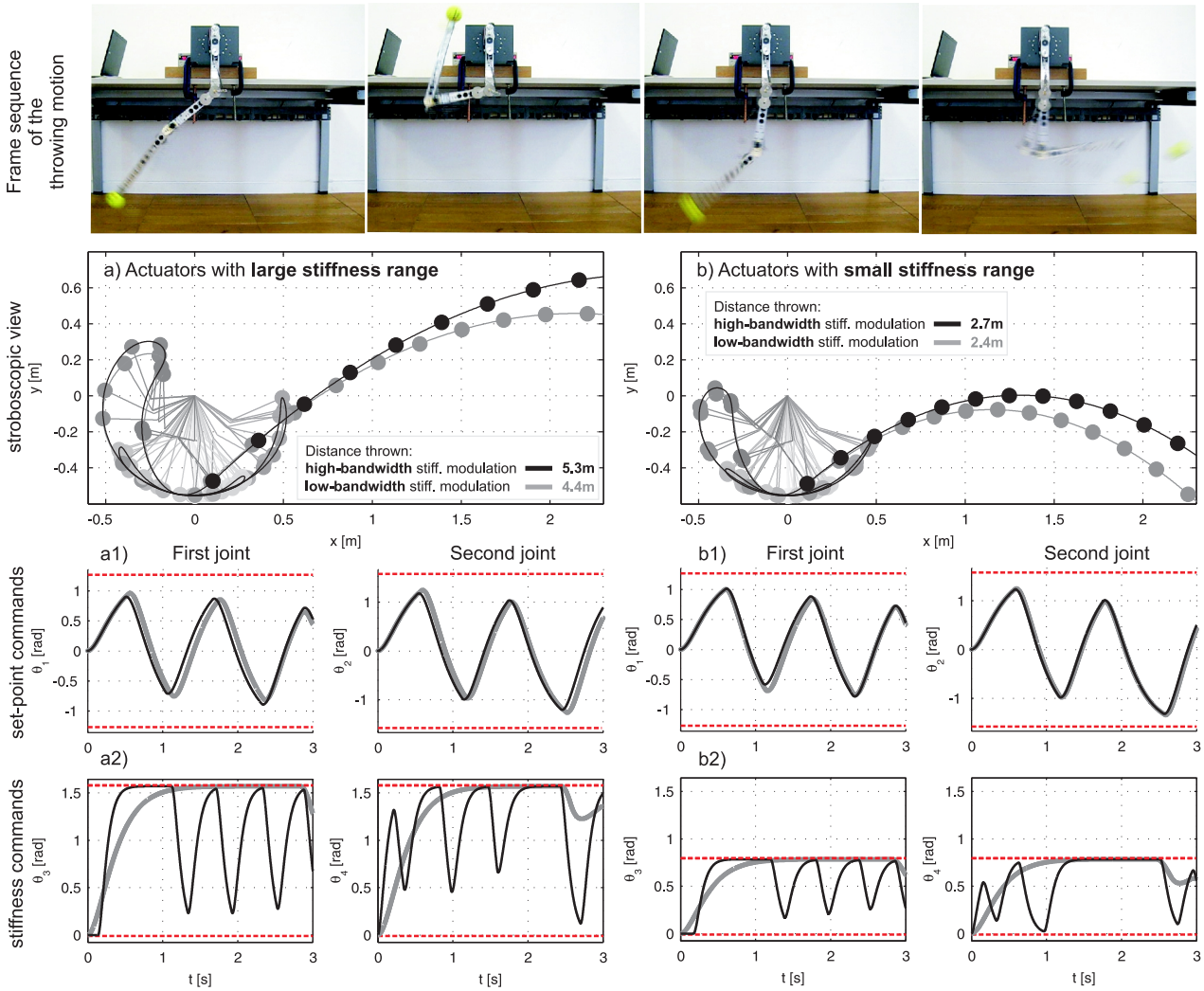

Fig. 4. Ball-throwing using: a1,a2) actuators having large stiffness range $\theta_{3,4} \in [0, \pi/2]$rad and high bandwidth $\boldsymbol{\alpha} = 5\text{diag}([1, 1, \sqrt{10}, \sqrt{10}])\text{s}^{-1}$ (black lines) or low bandwidth $\boldsymbol{\alpha} = 5\text{diag}([1, 1, 1, 10])\text{s}^{-1}$ (gray lines); b1,b2) actuators having small stiffness range $\theta_{3,4} \in [0, \pi/4]$rad and high bandwidth $\boldsymbol{\alpha} = 5\text{diag}([1, 1, \sqrt{10}, \sqrt{10}])\text{s}^{-1}$ (black lines) or low bandwidth $\boldsymbol{\alpha} = 5\text{diag}([1, 1, 1, 1])\text{s}^{-1}$ (gray lines). Limits on the motor positions (depicted with dashed red lines) are set to: $\theta_{1,2} \in [-2\pi/5, 2\pi/5]$rad. Practical implementation of the optimally planned motor program, corresponding to high-bandwidth and large stiffness range actuators (Fig.4a – black line), is demonstrated in the supplementary material. For further experiments on this system (and a similar one-link device) the reader is referred to [18] (and [16] respectively).

tion and Fig. 6b corresponding to a low bandwidth one. In Figs. 6a1,b1 one can see that the present formulation *enforces the state inequality limits, as hard constraints*. Figs. 6a2,b2 show that this is *non-trivial* since the boundaries of the constraints depend on stiffness modulation. Indeed, higher θ_3 and θ_4 in Figs. 6a3,b3 result in stronger restriction on ϕ_1 and ϕ_2 respectively. In Figs. 6a2,b2 one can also recognize a *bang-bang like strategy* (especially on the first joint). This strategy is planned under changing constraint boundaries and is *smooth* due to the bandwidth limitations of the actuators. Figs. 6a4,a5,b4,b5 show that neither of the constraints corresponding to the positions and velocities of the main motors (used to modulate the set-point of the virtual joint springs) are violated. *This result demonstrates the applicability of the present optimal control formulation under non-linear state inequality constraints that are often present as actuation constraints on robotic systems.*

2) Experiment: Using the proposed framework we computed and implemented one set of optimal motor trajectories corresponding to high bandwidth stiffness modulation realizing ball-throwing on the DLR-HASy. In Fig. 7 one can observe a good match between the simulated and the real link-side motions (i.e., $\mathbf{q}(t)$). This is partly because of an accurate system model, but also because the proposed optimization algorithm plans motor trajectories (i.e., $\boldsymbol{\theta}(t)$) that respect all physical constraints and as such can be precisely tracked on this complex system. In addition, and similar to the simulations in Fig. 6, we can see a characteristic counter movement action, initial back swing before rapid forward acceleration (Figs. 6a,b, please also see the multimedia material), and a similar stiffness modulation pattern despite the difference in dynamics (see Fig. 6a3) and constraints (see Fig. 7a2,b2). Moreover, we also recognize the characteristic sequential velocity peaks, first on the proximal link and then on the distal link Fig. 7a3,b3. These peaks are associated with the

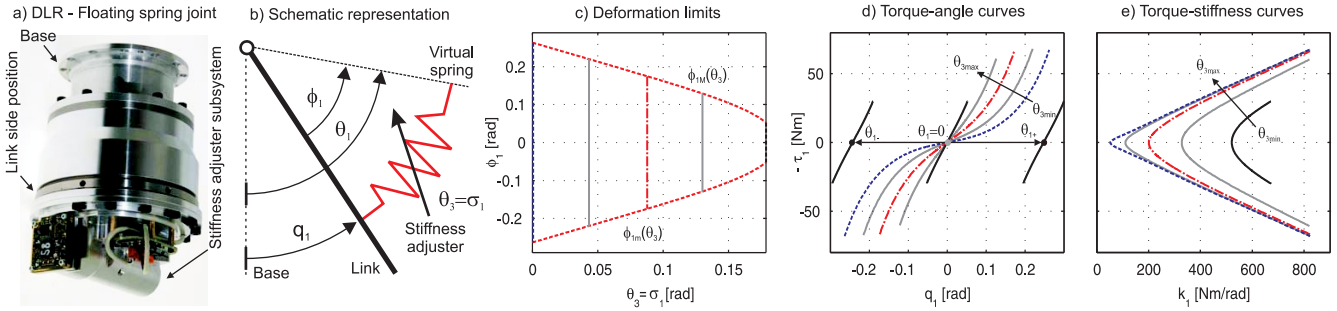

Fig. 5. a) The DLR floating spring joint (FSJ) [7]. b) Schematic representation: q_1 is the joint angle, θ_1 is the motor angle that is associated with the equilibrium position of the virtual rotational joint spring, $\phi_1 = \theta_1 - q_1$ is the length of the virtual spring while θ_3 is the motor angle that is associated with the stiffness of this spring. c) The deformation limit of the spring give rise to non-linear (stiffness command dependent) inequality constraints: $\phi_{1m}(\theta_3) \leq \phi_1 \leq \phi_{1M}(\theta_3)$. d) Torque-angle characteristics. e) Torque-stiffness characteristics. Note that, by setting $\theta_3 = c$, the DLR-FSJ behaves as a non-linear spring with controllable joint equilibrium angle θ_1, while by setting $\theta_1 = c$, it becomes a joint that could have different stiffness properties depending on θ_3. It is of practical interest to recognize that a *single* torque-stiffness curves indicates that the actuator is *not* capable of independent torque/stiffness modulation (i.e., SEA), while *multiple curves* (that enclose a region in the torque-stiffness plane – see Fig.3e and Fig.5e) indicate that *independent* torque/stiffness modulation is viable (i.e., VSA). Accordingly, *visual inspection of the torque-stiffness characteristics* may be used as an alternative to the analytical condition (19).

sequential (proximal-to-distal) motions of body segments often reported in human studies of striking and throwing skills [58].

3) Stiffness modulation: By means of stiffness modulation, we observe a characteristic decrease followed by a rapid increase of the stiffness just before the ball release ($t \approx 1s$, see Figs. 6a3,7a2,b2). This stiffness modulation strategy bears clear physical interpretation. Indeed, *decreased stiffness*, near to the end of the movement, enables the link to *maximally depart from its equilibrium configuration*. This then makes it possible to *accelerate the arm by increasing the stiffness* just before ball release. *This mechanism is predicted to be optimal on the present robotic system. Whether a similar mechanism is employed during human throwing and striking motions has yet to be investigated.*

It is important to recognize that a stiffness modulation strategy reported in Figs. 6a3,7a2,b2 is not possible in the case of fixed stiffness control [18] or when the bandwidth of the actuators associated with stiffness modulation is low, see Fig. 6b3. This leads to lower performance (i.e., shorter distance thrown, see Fig.6b).

4) Variable stiffness versus rigid actuation: Finally, we investigate how does the performance of the optimally controlled compliantly actuated robot (i.e., DLR HASy) compares to the best performance of the corresponding *rigid robot* (where $\dot{\mathbf{q}} = [\dot{\theta}_1, \dot{\theta}_2]^T$). To ensure a common ground for this comparison, we consider both systems to be subject to the same motor velocity limits i.e., $\dot{\theta}_1 \in [-3, 3]\text{rad/s}$ and $\dot{\theta}_2 \in [-3, 3]\text{rad/s}$ and also *assume no-torque limit on the rigid robot*[17]. *By comparing the link-side velocities, it becomes immediately clear that the same velocity peaks shown in Figs.7a3,b3 could not have been achieved with a rigid robot.* When reflected to the task performance, we found by kinematic calculation that while the rigid robot could, under no effort limitation, throw a ball $d = 3.6\text{m}$ (see Fig.8), the VS joints allowed the DLR HASy to throw a ball $d \approx 5\text{m}$. For the corresponding experimental video, the reader is referred to the multimedia attachment.

[17]This latter assumption makes the restrictions on the rigid robot weaker compared to those that apply on the DLR HASy where the elastic joint torques are limited, both in range and bandwidth.

This comparison shows the ability of the present optimal control framework to exploit the rigid body dynamics and the capacity of the compliant actuators to achieve better task performance. Moreover, it demonstrates the utility of optimal impedance control and the advantage of compliant design for the next generation of robotic systems.

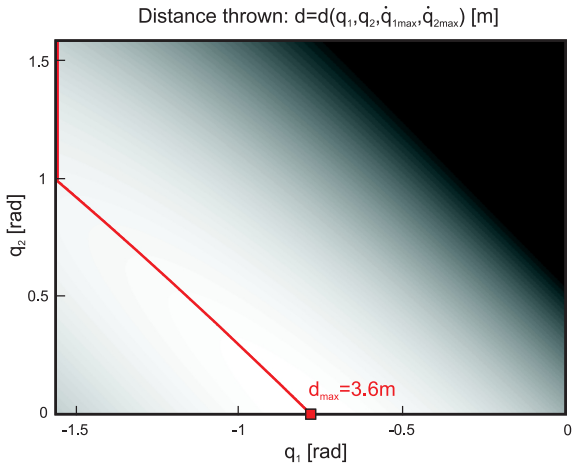

Fig. 8. Best throwing performance of a rigid robot as a function of the release configuration and under a given velocity limit: $\dot{\theta}_{1,2} \in [-3, 3]\text{rad/s}$ i.e., $\dot{\mathbf{q}}_{max} = [3, 3]^T\text{rad/s}$.

VIII. Conclusion

In this paper we provide an optimal-control formulation for compliantly actuated robots subject to actuation constraints. Instead of employing problem specific analytical derivations or using sophisticated numerical algorithms to treat the inequality constraints inevitably present on compliantly actuated robots, this formulation employs canonical box-constraints on control inputs to explicitly embed the actuation constraints into the dynamics. In practice, these actuation constraints can be range limits on the motor positions, bandwidth limitations due to the motor dynamics as well as deformation limits on the elastic elements inherent to many SEA and VSA designs. In this paper, we i) illustrate the impact of these limits

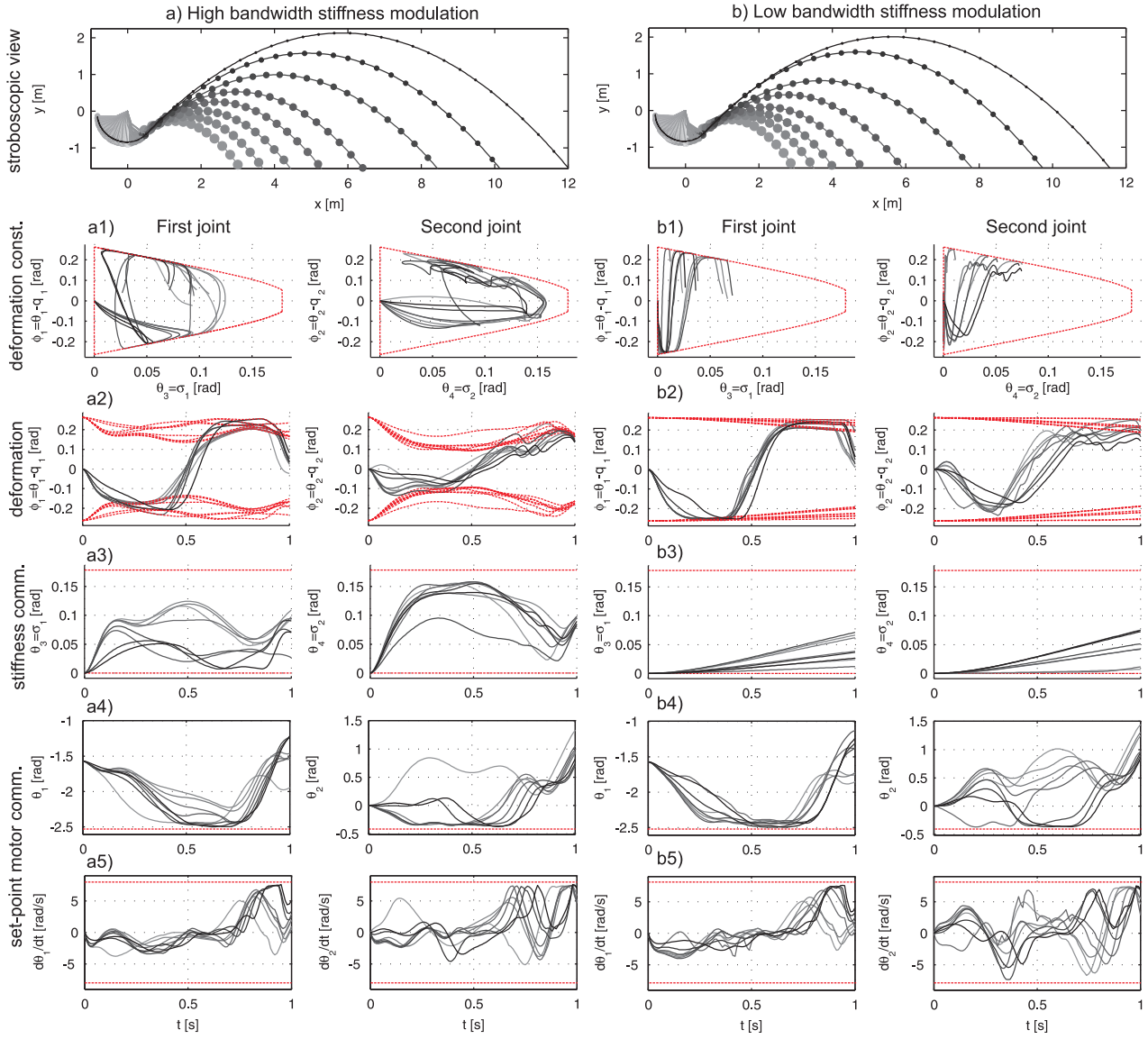

Fig. 6. Treatment of constraints: a) high-bandwidth stiffness modulation $\boldsymbol{\alpha} = \mathrm{diag}[25, 25, 15, 15]\mathrm{s}^{-1}$, b) low-bandwidth stiffness modulation $\boldsymbol{\alpha} = \mathrm{diag}[25, 25, 1.5, 1.5]\mathrm{s}^{-1}$. The simulations are performed with different ball masses: $m \in \{0.1, 1, 2, 3, 4, 5, 6, 7.26\}$kg (corresponding to black to light-gray lines) and fixed execution time: $T = 1$s. The limits on $\boldsymbol{\phi}$ are depicted with dashed red lines in Figs. 6a1,a2,b1,b2 while the constraints on $\theta_{3,4} = \sigma_{1,2} \in [0, 0.178]$rad are shown in Figs. 6a3,b3. In addition, we set: $\theta_1 \in [-1.05, 3.05]$rad, $\theta_2 \in [2.27, 0.44]$rad, $\dot{\theta}_{1,2} \in [-8, 8]\mathrm{rad/s}$ in these simulations as shown in Figs. 6a4,a5,b4,b5. In all cases, the throwing motion is started from a vertical hanging configuration with minimum stiffness. Note that in Figs. 6a1,b1 each solution (gray and black lines) strictly satisfies its own corresponding constraint (red dashed lines).

on the performance and the control strategy during optimal variable stiffness control and ii) demonstrate the viability of the proposed formulation on two conceptually different variable-stiffness system performing a dynamic task in simulations and experiments. The proposed framework may be further developed by integration of: i) a mechanism for *active feedback* control, to deal with unforeseen disturbances and environmental uncertainties and ii) a framework for *online dynamics adaptation*, to deal with systematic changes in the dynamics.

Finally, we note that this investigation has been partly motivated by the latest hardware developments in anthropomorphic robots, exoskeletons and prosthetic devices, where compliance is deliberately introduced into the system. In that regard, this work demonstrates the utility and viability of the proposed optimal control framework and provide some valuable design guidelines for the next generation of robotic devices where compliant actuation and variable impedance control is likely to play a dominant role.

IX. Appendix: Approaches to Constrained Optimization

Here we consider several *alternative* approaches that can be used to solve (43)–(45). The purpose of this section is to *highlight the benefits* of different methods and to *point out the practical difficulties* related to the treatment of complex (i.e., high-dimensional, non-linear and constrained) optimal control problems. For a more elaborate exposition on this matter the reader is referred to [45].

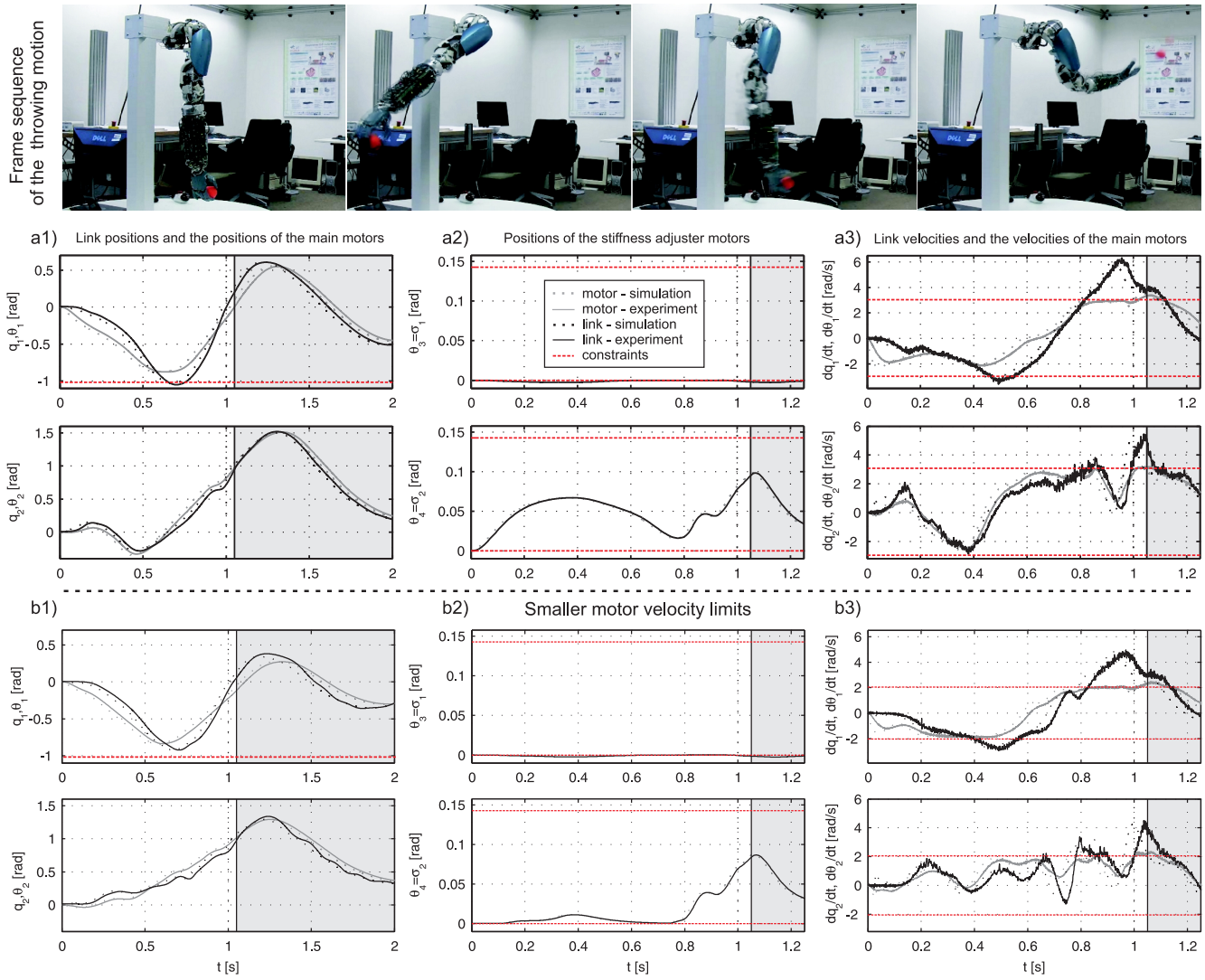

Fig. 7. Ball-throwing using optimal variable stiffness control: a1,b1) motor and link-side trajectories, a2,b2) stiffness adjustment, a3,b3) motor and link-side velocities. Both of these experiments are performed using a fixed execution time $T = 1s$ and a ball weighting $m = 0.06$kg. For the first experiment (a) the motor velocity limits are set to: $\dot{\theta}_{1,2} \in [-3, 3]$rad/s while for the second experiment (b) it was set to: $\dot{\theta}_{1,2} \in [-2, 2]$rad/s. The additional limits are defined by: $\theta_1 \in [-1.05, 3.05]$rad, $\theta_2 \in [2.27, 0.44]$rad, $\theta_{3,4} = \sigma_{1,2} \in 0.8[0, 0.178]$rad and $\boldsymbol{\alpha} = \text{diag}[25, 25, 15, 15]\text{s}^{-1}$. The throwing motion is started from a vertical hanging configuration with no initial velocity and minimum stiffness. In these experiments stiffness modulation is restricted to the second joint. For further experiments on this system, the reader may refer to [40].

A. *Indirect methods*

In an indirect approach, one attempts to find a solution that satisfies the *first order optimality conditions* to the original constrained functional minimization (43)–(45). For this purpose: i) the first order optimality conditions are derived using Pontryagin's maximum principle (PMP) [59], ii) these conditions are then represented with a *multi-point boundary value problem* (MPBVP) [44], and finally iii) the obtained MPBVP is solved using a *multiple-shooting method*, see [60]. The MPBVP generally contains the: state equations, adjoint equations, transversality conditions, differential equations that locate the entry and exit points for every state and control constrained sub-arcs and the associated jump conditions[18].

There are notable differences in this representation, and the corresponding solution, depending on whether state or only control constraints are considered. This is because *state inequalities* lead to *piecewise defined adjoint equations* and *discontinuous adjoint functions*. This complicates the treatment of state constrained formulations, partly because the discontinuities may lead to sensitivity/accuracy issues during numerical integration, but also because *the number of functions representing the piecewise defined adjoint equations has to be guessed*. Both of these issues can be circumvented using the present formulation that is subject to control constraints only.

Even if only control constraints are present, however, application of multiple-shooting methods generally requires the user to guess the *missing initial data* to integrate the adjoint equations, and to find the structure of the control constraint sub-arcs. This imposes strong restrictions, namely to make the numerical algorithm converge, *the user must generate a guess of the details of optimal solution.* [61].

[18]Erdmann-Weierstraß corner conditions [61].

B. Direct methods

In direct methods, one employs control and/or state parametrization to transform the original optimal control problem, e.g., (43)–(45), to a non-linear programming problem (NLP) [62]. Instead of finding a solution to the first order optimality conditions, the original infinite dimensional constrained *functional* minimization is directly converted to a finite dimensional *function* minimization that is easier to solve numerically. Indeed, such a function minimization can be solved using sophisticated NLP methods e.g., using sequential quadratic programming (SQP) [63].

There are numerous reasons that make this formulation attractive. One of these is that, direct methods do not require the optimality conditions to be analytically derived (that is often non-trivial and cumbersome for high-dimensional constrained problems). Moreover, unlike multiple shooting methods, non-linear programing is robust to initializations. Notably, for constrained problems, *non-linear programming can be applied without a prior specification of the sequence and number of constrained sub-arcs*. This is because the entry and exit points on these sub-arcs are automatically identified by standard *active set algorithms* [45].

On the other hand, however, control and state parameterization generally leads to a *large-scale* NLP. Due to this reason, exploiting the sparsity pattern of such a NLP is essential for *computationally tractable* implementation. Even if the computation is optimized in this way, there is a *natural trade-off between computational tractability and the accuracy of the solution* this approach provides. To circumvent possible accuracy issue, merging direct and indirect methods has been suggested [64]. Alternatively, successive approximation methods may also be employed.

C. Successive approximation methods

The idea of these methods is to derive a *sub-problem* that can be iteratively solved to improve the nominal control trajectory, initially provided by the user. Examples of these approaches are: Differential Dynamic Programming (DDP) [65], the iterative Linear Quadratic Regulator/Gaussian (iLQR/G) approach [53] as well as many other first and second order method derived from Bellman's dynamic programming or by using variational calculus [66]. Compared to direct methods, these iterative approaches provide more *precise solutions* while compared to indirect methods, these approaches are *robust against initializations*. In this light, many of the issues discussed above (e.g., computational efficiency, sensitivity to initialization, accuracy of the solution) could be addressed using methods for successive approximation. [67] provides a unified view of such approximation methods in the language of KL divergence minimisation. While these methods are primarily derived to solve unconstrained problems, there are also many alternatives when optimizing under state and control constraints [68].

In the present context, the state constraints are explicitly embedded in the dynamics, such that any method allowing box-constraints on controls would suffice. One of these methods is provided with the iLQR/G approach [53] that is applicable to non-linear problems and remains efficient for high-dimensional systems. This approach is used in Section VII.

REFERENCES

[1] M. Grebenstein, A. Albu-Schäffer, T. Bahls, M. Chalon, O. Eiberger, W. Friedl, R. Gruber, U. Hagn, R. Haslinger, H. Höppner, S. Jörg, M. Nickl, A. Nothhelfer, F. Petit, B. Pleintinger, J. Reil, N. Seitz, T. Wimböck, S. Wolf, T. Wüsthoff, and G. Hirzinger, "The DLR Hand Arm System," in *IEEE International Conference on Robotics and Automation*, (Shanghai, China), pp. 3175–3182, 2011.

[2] C. E. English, "Implementation of variable joint stiffness through antagonistic actuation using rolamite springs," *Mechanism and Machine Theory*, vol. 341, pp. 27–40, 1999.

[3] C. E. English and D. Russell, "Mechanics and stiffness limitations of a variable stiffness actuator for use in prosthetic limbs," *Mechanism and Machine Theory*, vol. 341, pp. 7–25, 1999.

[4] K. Koganezawa, Y. Watanabe, and N. Shimizu, "Antagonistic muscle-like actuator and its application to multi-DOF forearm prosthesis," *Advanced Robotics*, vol. 12, no. 7-8, pp. 771–789, 1999.

[5] G. Tonietti, R. Schiavi, and A. Bicchi, "Design and control of a variable stiffness actuator for safe and fast physical human/robot interaction," in *IEEE International Conference on Robotics and Automation*, (Barcelona, Spain), pp. 526–531, 2005.

[6] S. A. Migliore, E. A. Brown, and S. P. DeWeerth, "Novel nonlinear elastic actuators for passively controlling robotic joint compliance," *Journal of Mechanical Design*, vol. 129, no. 4, pp. 406–412, 2007.

[7] S. Wolf and G. Hirzinger, "A new variable stiffness design: Matching requirements of the next robot generation," in *IEEE International Conference on Robotics and Automation*, (Pasadena, CA, USA), pp. 1741 – 1746, 2008.

[8] R. van Ham, T. Sugar, B. Vanderborght, K. Hollander, and D. Lefeber, "Compliant actuator designs," *IEEE Robotics & Automation Magazine*, vol. 16, no. 3, pp. 81–94, 2009.

[9] A. Radulescu, M. Howard, D. J. Braun, and S. Vijayakumar, "Exploiting variable physical damping in rapid movement tasks," in *IEEE/ASME International Conference on Advanced Intelligent Mechatronics*, (Kaohsiung, Taiwan), pp. 141–148, July 2012.

[10] B. Siciliano and O. Khatib, *Handbook of Robotics*. Springer, 2008.

[11] N. Hogan, "Impedance control: An approach to manipulation," *ASME Journal of Dynamic Systems, Measurement and Control*, vol. 107, pp. 1–24, 1985.

[12] J. W. Hurst, J. Chestnutt, and A. A. Rizzi, "The actuator with mechanically adjustable series compliance," *IEEE Transactions on Robotics*, vol. 26, no. 4, pp. 597–606, 2010.

[13] B. Vanderborght, B. Verrelst, R. V. Ham, M. V. Damme, D. Lefeber, B. M. Y. Duran, and P. Beyl, "Exploiting natural dynamics to reduce energy consumption by controlling the compliance of soft actuators," *International Journal of Robotics Research*, vol. 25, no. 4, pp. 343–358, 2006.

[14] A. Bicchi and G. Tonietti, "Fast and soft arm tactics: Dealing with the safety-performance trade-off in robot arms design and control," *IEEE Robotics and Automation Magazine*, vol. 11, pp. 22–33, 2004.

[15] D. Mitrovic, S. Klanke, and S. Vijayakumar, "Learning impedance control of antagonistic systems based on stochastic optimization principles," *International Journal of Robotics Research*, vol. 30, no. 2, pp. 1–18, 2011.

[16] D. J. Braun, M. Howard, and S. Vijayakumar, "Exploiting variable stiffness in explosive movement tasks," in *Proceedings of Robotics: Science and Systems*, (Los Angeles, CA, USA), June-July 2011.

[17] S. Haddadin, M. Weis, S. Wolf, and A. Albu-Schäffer, "Optimal control for maximizing link velocity of robotic variable stiffness joints," in *IFAC World Congress*, (Milano, Italy), August-September 2011.

[18] D. J. Braun, M. Howard, and S. Vijayakumar, "Optimal variable stiffness control: Formulation and application to explosive movement tasks," *Autonomous Robots*, vol. 33, no. 3, pp. 237–253, 2012.

[19] M. Spong, "Modeling and Control of Elastic Joint Robots," *Journal of Dynamic Systems, Measurement, and Control*, vol. 109, no. 4, pp. 310–319, 1987.

[20] P. Tomei, "A simple PD controller for robots with elastic joints," *IEEE Transactions on Automatic Control*, vol. 36, no. 10, pp. 1208–1213, 1991.

[21] G. Pratt and M. Williamson, "Series elastic actuators," in *IEEE/RSJ International Conference on Intelligent Robots and Systems*, vol. 1, (Pittsburg, PA), pp. 399–406, 1995.

[22] A. DeLuca, F. Flacco, A. Bicchi, and R. Schiavi, "Nonlinear decoupled motion-stiffness control and collision detection/reaction for the VSA-II variable stiffness device," in *IEEE/RSJ International Conference on Intelligent Robots and Systems*, (St. Louis, USA), pp. 5487–5494, October 2009.

[23] A. Albu-Schäffer, S. Wolf, O. Eiberger, S. Haddadin, F. Petit, and M. Chalon, "Dynamic modelling and control of variable stiffness actuators," in *IEEE International Conference on Robotics and Automation*, (Anchorage, Alaska), pp. 2155–2162, May 2010.

[24] D. J. Braun, F. Petit, F. Huber, S. Haddadin, P. Smagt, A. Albu-Schäffer, and S. Vijayakumar, "Optimal torque ans stiffness control in compliantly actuated robots," in *IEEE/RSJ International Conference on Intelligent Robots and Systems*, (Vilamoura, Portugal), pp. 2801–2808, October 2012.

[25] B. Brogliato, R. Ortega, and R. Lozano, "Global tracking controller for flexible-joint manipulators: A comparative study," *Automatica*, vol. 31, no. 7, pp. 941–956, 1995.

[26] M. W. Spong, K. Khorasani, and P. V. Kokotović, "An integral manifold approach to the feedback control of flexible joint robots," *IEEE Journal of Robotics and Automation*, vol. RA-3, no. 4, pp. 291–300, 1987.

[27] A. DeLuca, "Feedforward/feedback laws for the control of flexible robots," in *IEEE International Conference on Robotics and Automation*, (San Francisco, CA, USA), pp. 233–240, April 2000.

[28] S. Nicosia and P. Tomei, "A method to design adaptive controllers for flexible joint robots," in *IEEE International Conference on Robotics and Automation*, vol. 1, pp. 701–706, May 1992.

[29] A. Albu-Schäffer and G. Hirzinger, "A globally stable state-feedback controller for flexible joint robots.," *Journal of Advanced Robotics*, vol. 15, no. 8, pp. 799–814, 2001.

[30] C. Ott, A. Albu-Schäffer, A. Kugi, and G. Hirzinger, "On the passivity-based impedance control of flexible joint robots," *IEEE Transactions on Robotics*, vol. 24, no. 2, pp. 416–429, 2008.

[31] G. Palli, C. Melchiorri, T. Wimbock, M. Grebenstein, and G. Hirzinger, "Feedback linearization and simultaneous stiffness-position control of robots with antagonistic actuated joints," in *IEEE International Conference on Robotics and Automation*, (Roma, Italy), pp. 4367–4372, May 2007.

[32] G. Palli, C. Melchiorri, and A. D. Luca, "On the feedback linearization of robots with variable joint stiffness," in *IEEE International Conference on Robotics and Automation*, (Pasadena, CA, USA), pp. 1753–1759, May 2008.

[33] L. Ljung, *System Identification: Theory for the User*. N.J. USA: Prentice-Hall, Upper Saddle River, 1999.

[34] S. Vijayakumar, A. D'Souza, and S. Schaal, "Incremental online learning in high dimensions," *Neural Computation*, vol. 17, pp. 2602–2634, 2005.

[35] D. Mitrovic, S. Klanke, and S. Vijayakumar, "Adaptive optimal feedback control with learned internal dynamics models," *In: From Motor Learning to Interaction Learning in Robots, Springer-Verlag*, vol. SCI-264, pp. 65–84, 2010.

[36] K. J. Salisbury, "Active stiffness control of a manipulator in cartesian coordinates," in *Proceedings of the 19th IEEE Conference on Decision and Control*, vol. 19, pp. 95–100, December 1980.

[37] N. Hogan, "Impedance control of industrial robots," *Robotics and Computer-Integrated Manufacturing*, vol. 1, no. 1, pp. 97–113, 1984.

[38] M. Uemura and S. Kawamura, "Resonance-based motion control method for multi-joint robot through combining stiffness adaptation and iterative learning control," in *IEEE International Conference on Robotics and Automation*, (Kobe, Japan), pp. 1543 – 1548, 2009.

[39] M. Garabini, A. Passaglia, F. A. W. Belo, P. Salaris, and A. Bicchi, "Optimality principles in variable stiffness control: the VSA hammer," in *Proceedings of the IEEE/RSJ International Conference on Intelligent Robots and Systems*, (San Francisco, USA), September 2011.

[40] S. Haddadin, F. Huber, and A. Albu-Schäffer, "Optimal control for exploiting the natural dynamics of variable stiffness robots," in *IEEE International Conference on Robotics and Automation*, (St Paul, MN, USA), pp. 3347–3354, 2012.

[41] J. Nakanishi and S. Vijayakumar, "Exploiting passive dynamics with variable stiffness actuation in robot brachiation," in *Robotics: Science and Systems*, (Sydney, Australia), 2012.

[42] J. E. Bobrow, S. Dubowsky, and J. S. Gibson, "Time-optimal control of robotic manipulators along specified paths," *The International Journal of Robotics Research*, vol. 4, no. 3, pp. 3–17, 1985.

[43] D. S. Bernstein and A. N. Michel, "A chronological bibliography on saturating actuators," *International Journal of Robust and Nonlinear Control*, vol. 5, pp. 375–380, 1995.

[44] H. J. Pesch, "A practical guide to the solution of real-life optimal control problems," *Control and Cybernetics*, vol. 23, no. 1, pp. 7–60, 1994.

[45] J. T. Betts, "Survey of numerical methods for trajectory optimization," *AIAA Journal of Guidance, Control and Dynamics*, vol. 21, no. 2, pp. 193–207, 1998.

[46] A. DeLuca, B. Siciliano, and L. Zollo, "PD control with on-line gravity compensation for robots with elastic joints: Theory and experiments," *Automatica*, vol. 41, pp. 1809–1819, 2005.

[47] H. Goldstein, *Classical Mechanics*. Addison-Wesley, 1980.

[48] G. Golub and C. V. Loan, *Matrix Computations*. The John Hopkins University Press, 3 ed., 1996.

[49] W. Rudin, *Principles of Mathematical Analisys*. McGraw-Hill Inc. New York, 3 ed., 1953.

[50] C. T. Kelley, *Solving Nonlinear Equations with Newton's Method*. SIAM, 2003.

[51] M. Goldfarb and T. Sirithanapipat, "The effect of actuator saturation on the performance of PD-controlled servo systems," *Mechatronics*, vol. 9, pp. 497–511, 1999.

[52] W. L. Nelson, "Physical principles for economies of skilled movements," *Biological Cybernetics*, vol. 46, no. 2, pp. 135–147, 1983.

[53] W. Li and E. Todorov, "Iterative linearization methods for approximately optimal control and estimation of non-linear stochastic system," *International Journal of Control*, vol. 80, no. 9, pp. 1439–1453, 2007.

[54] R. van Ham, B. Vanderborght, M. V. Damme, B. Verrelst, and D. Lefeber, "MACCEPA, the mechanically adjustable compliance and controllable equilibrium position actuator: Design and implementation in a biped robot.," *Robotics and Autonomous Systems*, vol. 55, no. 10, pp. 761–768, 2007.

[55] N. Hogan, "Adaptive control of mechanical impedance by coactivation of antagonist muscles," *IEEE Transactions on Automatic Control*, vol. AC-29, no. 8, pp. 681–690, 1984.

[56] J. M. Winters and L. Stark, "Analysis of fundamental human movement patterns through the use of in-depth antagonistic muscle models," *IEEE Transactions on Biomedical Engineering*, vol. BME-32, pp. 826–839, 1985.

[57] M. Howard, D. J. Braun, and S. Vijayakumar, "Transferring human impedance behaviour to heterogeneous variable impedance actuators," *IEEE Transactions on Robotics*, 2013 - in press.

[58] C. Putnam, "Sequential motions of body segments in striking and throwing skills: descriptions and explanations," *Journal of Biomechanics*, vol. 26, no. 1, pp. 125–135, 1993.

[59] L. S. Pontryagin, V. G. Boltyanskii, R. V. Gamkrelidze, and E. F. Mishchenko, *The Mathematical Theory of Optimal Processes*. John Wiley and Sons, New York, 1962.

[60] U. Ascher, R. Mattheij, and R. D. Russell, *Numerical solution of Boundary Value Problems for Differential Equations*. SIAM, 1988.

[61] A. E. Bryson and Y. C. Ho, *Applied Optimal Control*. Hemisphere, Wiley, 1975.

[62] C. R. Hargraves and S. W. Paris, "Direct trajectory optimization using nonlinear programming and collocation," *Journal of Guidance Control and Dynamics*, vol. 10, pp. 338–342, 1987.

[63] P. E. Gill, W. Murray, M. A. Saunders, and M. H. Wright, *User's guide for NPSOL (version 4) Report SOL 86-2*. Department of Operations Research, Stanford University, California, USA, 1986.

[64] O. von Stryk and R. Bulirsch, "Direct and indirect methods for trajectory optimisation," *Annals of Operations Research*, vol. 37, pp. 357–373, 1992.

[65] D. H. Jacobson and D. Q. Mayne, *Differential Dynamic Programming*. New York: Elsevier, 1970.

[66] D. H. Jacobson, "Second-order and second-variation methods for determining optimal control: A comparative study using differential dynamic programming," *International Journal of Control*, vol. 7, no. 2, pp. 175–196, 1968.

[67] K. Rawlik, M. Toussaint, and S. Vijayakumar, "On stochastic optimal control and reinforcement learning by approximate inference," in *Proceedings of Robotics: Science and Systems*, (Sydney, Australia), 2012.

[68] S. J. Yakowitz, "The stagewise Kuhn-Tucker condition and differential dynamic programming," *IEEE Transactions on Automatic Control*, vol. AC-31, no. 1, pp. 25–30, 1986.

David J. Braun (M'09) earned his Ph.D. ('06-'09) in Mechanical Engineering from Vanderbilt University. Following that he was affiliated with the Center for Intelligent Mechatronics (CIM) at Vanderbilt, conducted research at the German Aerospace Center (DLR) and is currently a postdoctoral research fellow at the University of Edinburgh. His research interests include system dynamics, nonlinear optimal control, impedance control and variable impedance actuation.

Florian Petit received the Dipl.-Ing. degree in electrical engineering from the Technical University of Munich (TUM), Munich, Germany, in 2008. He joined the Institute of Robotics and Mechatronics, German Aerospace Center (DLR), Wessling, Germany, in 2009. He is also member of the Sensory-Motor Systems Laboratory, Swiss Federal Institute of Technology Zurich (ETHZ), Zurich, Switzerland, since 2012. His research interests include variable impedance robots and control, impedance and force control, and nonlinear systems and control.

Felix Huber received his Dipl.-Ing. degree in Mechatronics in 2012 from Johannes Kepler University in Linz, Austria. He currently works at the Institute of Robotics and Mechatronics at the German Aerospace Center (DLR) as a Research Engineer. His research interests include robot modeling and control, and optimization.

Sami Haddadin (M'10) received his Ph.D. summa cum laude in 2011 from RWTH Aachen. He coordinates DLRs "HumanCentered Robotics" group and is lecturer at TUM. His research interests include pHRI, real-time planning, control and learning, VIA, optimal control, and safety. He organized and was PC member/editor of several workshops and conferences. He received six ICRA/IROS awards, the 2012 George Giralt Best Ph.D. Thesis Award, the TRO 2011 Best Paper Award, and was finalist of the Robotdalen Science Award 2009. He was guest editor of IJRR and has published more than 65 papers/chapters in journals, books, and conferences.

Patrick van der Smagt (M'12) focuses his research on biomimetic robotics and machine learning, and their application to assistive robotics and rehabilitation. After finishing his Ph.D. in Amsterdam, he joined DLR's robotic institute and, as head of bionic robotics, left for a professorship at the computer science faculty of the Technische Universitt Mnchen. Patrick tries to follow nature as a teacher.

Alin Albu-Schäffer (M'93) received his Diploma Degree in electrical engineering from the technical University of Timisoara, Romania in 1993 and the Ph.D. degree in Control Systems in 2002 from the Technical University of Munich, Germany. Since 2012 he is the head of the Institute of Robotics and Mechatronics at the German Aerospace Center (DLR), which he joined in 1995. His research interests include robot design, modeling, and control, nonlinear control, flexible joint and variable compliance robots, impedance and force control, physical human-robot interaction.

Sethu Vijayakumar is the Professor of Robotics and the Director of the Institute of Perception, Action and Behavior in the School of Informatics at the University of Edinburgh, where he holds the Royal Academy of Engineering Microsoft Research Chair in Learning Robotics. He also has additional appointments as an Adjunct Faculty of the University of Southern California, Los Angeles and a Visiting Research Scientist at the RIKEN Brain Science Institute, Tokyo. He has a Ph.D. (1998) in Computer Science and Engineering from the Tokyo Institute of Technology. His research interests span a broad interdisciplinary curriculum ranging from statistical machine learning, robotics, planning and optimization in autonomous systems to human motor control and optimality. He is a Fellow of the Royal Society of Edinburgh.